8-2012

Fault Analysis Of An Unbalanced Distribution System With Distributed Generation

Parimal Saraf
Clemson University, psaraf@g.clemson.edu

FAULT ANALYSIS OF AN UNBALANCED DISTRIBUTION SYSTEM WITH DISTRIBUTED GENERATION

A Thesis
Presented to
the Graduate School of
Clemson University

In Partial Fulfillment
of the Requirements for the Degree
Master of Science
Electrical Engineering

---

by
Parimal Saraf
August 2012

Accepted by:
Dr. Elham Makram, Committee Chair
Dr. Rajendra Singh
Dr. Richard Groff

ABSTRACT

In recent years there has been a lot of emphasis on renewable power integration due to environmental issues and to lower the dependence on fossil fuels. The presence of renewable sources in the distribution systems adds complexity to the calculation of the power flows and hence has a direct impact on the short circuit calculations, protection and control. The presence of unbalance in distribution systems worsens the situation since the three phase voltages and currents are no longer equal in magnitude and 120^{o} phase shifted.

This thesis involves a fault study in a 14-bus distribution system with integrated wind and solar power generation and shows the impact of unbalance in the system on short circuit calculations. The effect of unbalance on the behavior of traditional synchronous sources is already known and has been shown to cause errors in fault current magnitudes in the system. This thesis aims at observing and comparing the behavior of distributed generators in a balanced and an unbalanced distribution system. Detailed modeling of the DFIG and a grid connected PV array has been carried out in PSCAD. A 14 bus distribution system has been built and the distributed sources have been integrated into it. Unbalance has been introduced into an originally built balanced system by applying unbalanced loads at the buses and using untransposed feeders. Therefore, two systems, balanced and unbalanced, have been simulated and the behavior of the integrated distributed sources during faults has been compared for both the cases.

ACKNOWLEDGEMENTS

I wish to express my gratitude to my adviser, Dr. Elham Makram for her guidance, support, kindness and patience throughout the period of research and study at Clemson University.

I want to thank late Dr. Adly Girgis for being an exceptional teacher and a role model.

I thank Dr. Rajendra Singh and Dr. Richard Groff for their patience and acceptance to be my committee members.

I thank all the fellow students in my group, especially Chaoqi Ji and Harkaran Grewal, with whom I had a lot of fruitful discussions throughout the course of my period at the university.

I thank the Department of Electrical and Computer Engineering and the professors with whom I worked through the course of my masters. They helped develop and improve my knowledge of electrical engineering.

Last but not the least I want to thank my parents, grandparents and sister who have always been encouraging and patient.

TABLE OF CONTENTS

LIST OF FIGURES

List of Figures (Continued)

LIST OF TABLES

List of Tables (Continued)

CHAPTER 1

INTRODUCTION

Electric energy is one of the most highly consumed sources of energy. Almost all daily life applications consume electric power in one form or other. Exponential growth of population and industries has led to an increase in power consumption over a period of time. This in turn has led to increased consumption of fossil fuels that have been the main sources of power generation for decades. This dependency on fossil fuels affects the cost of power generation as fuel prices keep on varying all the time. Moreover, the power generation from fossil fuels amounts to 24% of the total greenhouse emissions [1]. The authors have also predicated a 77% increase in power consumption by the year 2030 that requires an increase in generation of about 4800 GW in the next decade [1]. In order to keep the emissions under control and at the same time meet the increasing electricity demand, a significant development has to be made in the area of distributed generation. Distributed generation by definition refers to limited size generation (typically 10MW or less) integrated to the substation, distribution feeders or residential loads [2]. Due to advancements in the area of renewable energy integration, very large scale integration is being carried out and currently the biggest wind farm in the US generating almost 750 MW [3] and a solar farm generating 45 MW [4] have been established. Figure 1.1 shows a generalized view of distributed generation integrated to the main electricity grid.

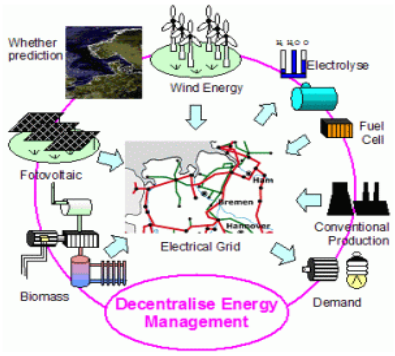

Figure 1.1 Decentralized or distributed generation [5]

There are a plenty of factors that prevent the widespread installation of renewable sources. Limited transmission capacity in many countries is one of the primary factors that affect their installation. The cost of installation is another major issue and therefore, the willingness of utilities to invest money is an important factor. Both wind and solar power generation facilities require a considerable amount of initial investment but there is no fuel cost involved unlike the generation based on fossil fuels or nuclear energy.

Although the power generated from renewable sources has issues of scheduling and reliability associated with it, but continuous advancements are being made in the area of renewable energy integration to the grid due to the fuels involved being inexhaustible and environment friendly. Wind and solar power generation are undoubtedly the most widely used and developed sources of renewable power generation today. The power generation from wind and solar has increased from a few kilowatts to several megawatts today. Constant research and development in the areas of wind and solar power generation have increased the reliability associated with these sources and in turn resulted in reduction of the cost of generation associated with them.

1.1 Wind power generation

Wind generators can be used either as standalone generators (residential and industrial application) or grid connected generators depending on the type of application. The type of generators used for wind power generation can be classified, based on the operating speed and architecture, as [6]:

a) Type A: These are squirrel cage induction generators that operate at just one speed.

b) Type B: These kinds of generators involve wound rotor induction generators and allow a narrow variable speed operation due to the presence of resistors connected to the rotor. Both A and B type generators are used for industrial and residential applications.

c) Type C: These kinds of generators allow variable speed operation and the rotor has terminals that are connected to the grid using an AC/DC/AC converter.

d) Type D: These kinds of generators allow variable speed operation and better power control as the AC/DC/AC converter is connected directly in front of the stator. The only disadvantage is that this class of generators requires a bigger size of AC/DC/AC converter.

The ability of type C and D wind turbines to extract maximum power under variable wind conditions and their excellent real and reactive power controllability make them favorable for utility scale applications. Figure 1.2 presents all four kinds of wind generator configurations mentioned previously.

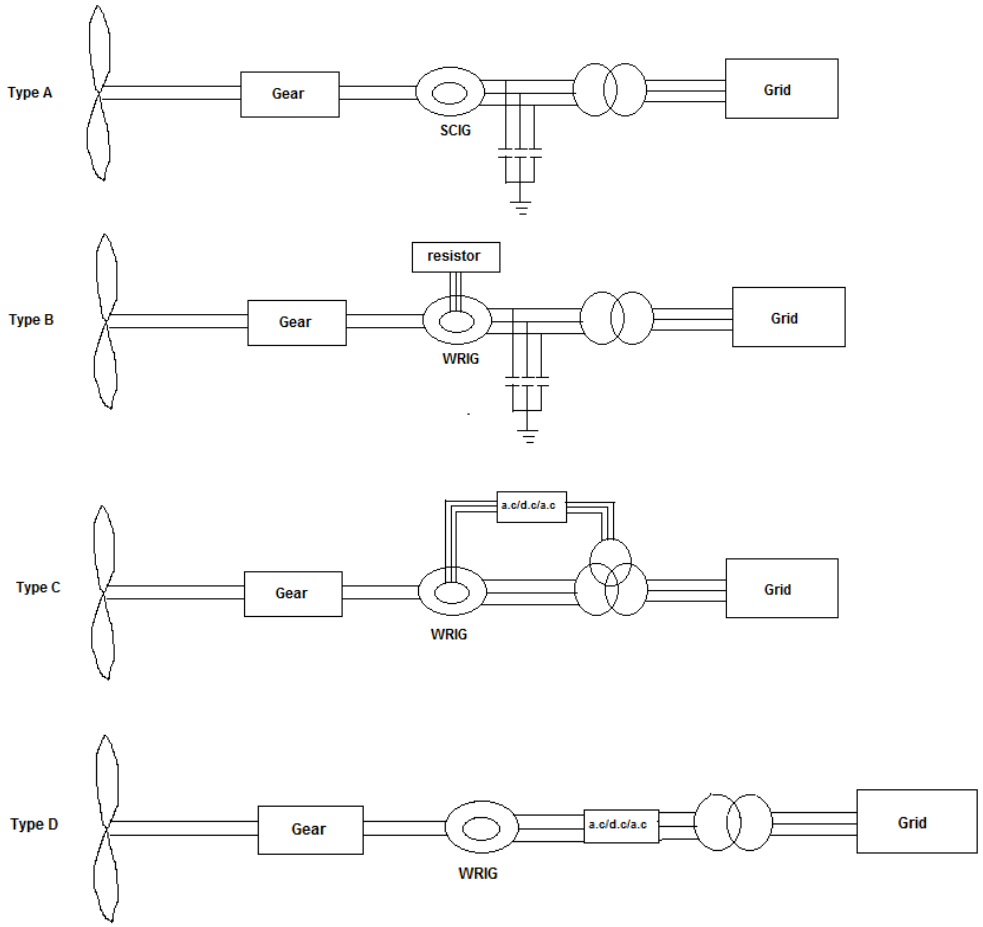

Figure 1.2 various types of wind generator configurations [6]

SCIG is squirrel cage induction generator; WRIG is wound rotor induction generator

1.1.1 DFIG basics and literature review

The most commonly used type of generator for wind power generation is a Doubly Fed Induction Generator (DFIG) which is also synonymous to type C wind generator configuration. DFIG enables the extraction of maximum power available in the wind, it has the capability to operate over a range of wind speeds (±30% slip) and it can control power in a flexible way. A grid connected DFIG involves a wound rotor induction

machine and has terminals on both stator and rotor. In other words, DFIG can exchange power from both stator and rotor side. But being an induction machine, the rotor frequency is dependent on the operating slip of the machine. So, an AC/DC/AC converter is used to connect the rotor terminals to the grid. The AC/DC/AC converter enables the variable speed operation and also makes the output real and reactive power controllable [6].

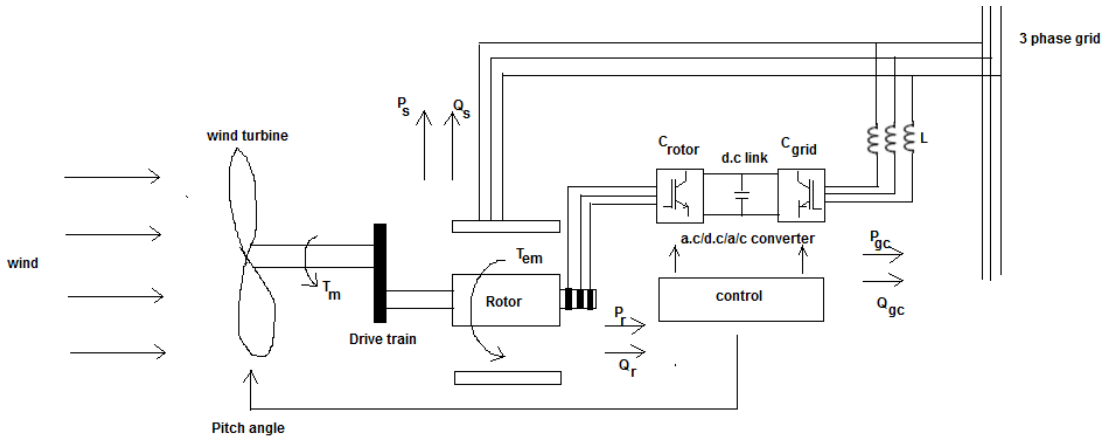

Figure 1.3 Power flow in the DFIG [7]

The DFIG can operate in sub-synchronous (when $\omega_m<\omega_1$) and super-synchronous modes ($\omega_m>\omega_1$). In sub-synchronous mode, the power flows from the grid into the rotor, i.e., rotor consumes power and in super-synchronous speed, the power flows from the rotor into the grid, i.e., the rotor supplies power to the grid [7].

The FERC regulation 661-A [8] states that the DFIG based wind parks cannot operate at power factors below 0.95 leading or lagging. Based on the regulation, the wind parks are operated close to unity power factor. References [9, 10] contain detailed modeling of

induction machines in d-q axis reference frames. References [11, 12, 13, 14] have given detailed description of the implementation of vector control of rotor-side and grid-side converters. The purpose of the rotor side converter is to control the real and reactive power exchange between the stator and the grid whereas the purpose of the grid side converter is to keep the DC link voltage constant.

One of the major technical issues associated with renewable energy integration is that it affects the fault current magnitudes in the system. The presence of multiple generators makes the distribution system non-radial and the fault current is supplied by multiple sources instead of a single source. The integration of large amounts of renewable power ranging in megawatts will surely supply a considerable amount of fault current during faults and hence have a heavy impact on protection schemes.

Reference [15] has shown the behavior of DFIG during faults. The paper has showed the fault current and voltage waveforms for all kinds of faults applied at various locations in a system with nine megawatts of wind generation (six 1.5 MW DFIGs). The authors have shown through simulations that the fault current transients and magnitudes are higher when the faults are closer to the wind farm. Reference [16] has shown the fault current contribution for all types of wind generators including DFIG. The work is focused mainly on the current transient during faults supplied by the wind generator. Reference [17] has shown that large scale integration of distributed generators in distribution system affects the coordination settings between protective devices. In [18], the authors have shown through an example that the coordination between fuses and re-closers is affected

due to the presence of distributed generators and have proposed an adaptive protection algorithm for better protection of such systems.

1.2 Solar power generation

1.2.1 Solar cell model

A solar cell can be modeled as a current source with an anti-parallel diode, a series resistance and a shunt resistance . Figure 1.4 shows the equivalent circuit of a single solar cell.

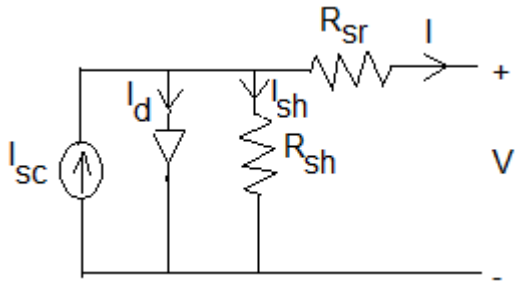

Figure 1.4 Equivalent circuit of a PV cell

The current generated by the current source, I_{sc} depends on the solar irradiance and the cell temperature at any given time. The I-V characteristic of a solar cell has been shown in figure 1.5 below. The figure also shows the maximum power point on the curve and $V_{m.p.p}$ represents the maximum power point voltage.

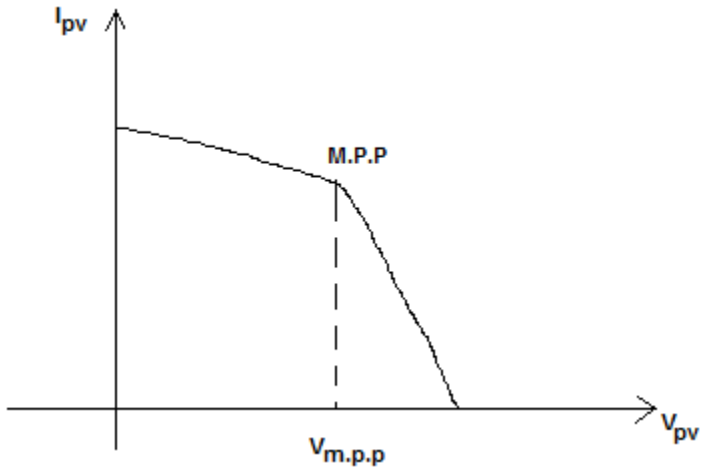

Figure 1.5 I-V characterstic of a PV cell [19]

The output current I delivered by a solar cell can be given as [19]:

$$I = I_{sc} - I_o\left[\exp\left(\frac{V + IR_{sr}}{nkT_c/q}\right) - 1\right] - \left(\frac{V + IR_{sr}}{R_{sh}}\right)$$

$$I_{sc} = I_{scR}\frac{G}{G_R}[1 + \alpha_T(T_c - T_{cR})]$$

$$I_o = I_{oR}\left(\frac{T_c^3}{T_{cR}^3}\right)\exp\left[\left(\frac{1}{T_{cR}} - \frac{1}{T_c}\right)\frac{qe_g}{nk}\right]$$

Where I_{sc} is the short circuit current, I_{scR} is the short circuit current at reference temperature, I_o is the dark current, I_{oR} is the dark current at reference cell temperature, α_T refers to the temperature coefficient of the cell, n is the diode ideality factor which is typically between 1 and 2 and depends on the material of the solar cell, G is the amount of solar radiation at the existing cell temperature, G_R is the amount of solar radiation at

reference temperature, k is the boltzmann's constant, q is the charge of an electron, e_g is the band gap energy and depends on the material of the solar cell, T_c is the existing cell temperature and T_{cR} is the reference cell temperature.

1.2.2 Grid connected photovoltaic generator basics and literature review

Any number of solar cells can be connected in series or parallel to form a solar array. A large solar array can produce enough power to be integrated to the grid. An important feature of a solar cell or an array is the maximum power point tracking (MPPT). There is an optimum operating point on the I-V curve of a solar array that represents the maximum power production point of the array known as the maximum power point. An MPP tracker can be used to track the maximum power point on the I-V curve under any given solar radiation and cell temperature. A dc-dc boost converter is normally used for the purpose of tracking the maximum power point voltage. The boost converter keeps the voltage across the capacitor C_1 shown in figure 1.6 constant at the maximum power point voltage. A simple P and Q control has been implemented for controlling the real and reactive power exchange between the PV system and the grid [19]. The circuit showing a grid connected PV system has been presented in figure 1.6 below.

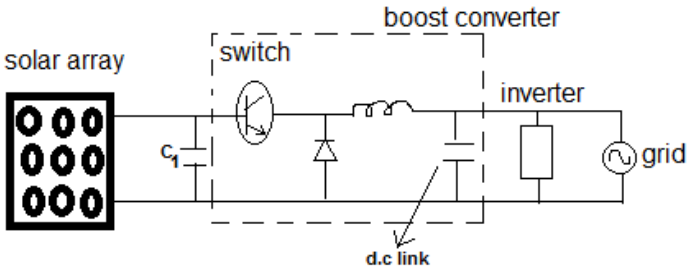

Figure 1.6 Grid connected photovoltaic generator

1.3 Unbalance in distribution systems

The transmission systems in the electric power network are usually balanced and the phase voltages are equal in magnitude and 120^{o} apart. Unlike the transmission systems, distribution systems are always unbalanced due to the presence of unbalanced loads and unequal mutual coupling between feeders. The application of the analysis techniques, developed for transmission systems, to distribution systems result in a lot of errors in steady state and transient calculations. Reference [20] has studied the causes and effects of voltage unbalance in distribution systems and suggested mitigation techniques for the same.

Separate analysis techniques have been developed for the steady state and transient analysis of unbalanced distribution systems such as three phase load flow, bus impedance matrix for fault analysis etc. Reference [21] has used the bus impedance matrix for analyzing open-conductor and shunt faults. The paper has showed that the error in calculation of fault currents in the unbalanced system under study using symmetrical components method varies between 10% and 20% depending on the type of fault. Reference [22] has shown the effect of gradual increase of load unbalance and fault resistance on fault current magnitudes. Reference [23] has shown the error that arises in fault current magnitudes using symmetrical component method in IEEE standard 13, 34 and 123 bus distribution systems. The authors of reference [23] have concluded that the amount of error depends on the degree of unbalance rather than the size of the system.

Reference [24] has shown the impact of unbalance in distribution systems on the transient stability of the induction motors. The authors have studied the behavior of

induction motors in a distribution system with various combinations of unbalanced feeder and unbalanced loading. Fault studies have been carried out for the system under various scenarios and it has been found that a double line to ground fault in the system with an unbalanced feeder is the worst condition for transient stability of the induction motor.

1.4 Organization of the thesis

The thesis starts with the development of control schemes for wind and solar generators in PSCAD followed by their interconnection to the grid and the fault analysis. The second chapter gives the detail of the implementation of the control system for a DFIG. Similarly, chapter three elaborates the control system implementation for a three phase grid connected photovoltaic system. The steady state operation of the DFIG as well as the grid connected photovoltaic system is very important for ensuring appropriate results of peak current magnitudes during faults. Therefore, both the chapters have the plots for steady state power, voltage and currents at the end to demonstrate that the control system implemented works perfectly. Chapter four has a brief description of the distribution system and also has the results comparing the fault current magnitudes supplied by the distributed generators in the balanced and unbalanced systems. Chapter five lists the conclusions of this thesis as well as the possible future work.

CHAPTER 2

GRID CONNECTED WIND GENERATION: CONTROL AND IMPLEMENTATION IN PSCAD

2.1 Introduction

This chapter covers the implementation of the control scheme of the DFIG. The DFIG consists of two three phase power electronic converters namely grid side and rotor side converter. Both the converters are responsible for controlling the real and reactive power exchange between the machine and the grid. Therefore, the control of both the converters is very vital for ensuring good performance of the machine. The chapter illustrates the performance of the control at the end of the chapter by showing the plots for the steady state voltage, current and powers supplied by the DFIG.

2.2 Wind turbine

The wind turbine extracts the kinetic energy from the wind and converts it into mechanical energy that in turn rotates the rotor of the wind generator and generates electricity. The mechanical power output of the turbine shaft is given as [6]:

$$P_m = \frac{1}{2}\rho_{air} A_{blade} C_p(\beta, \lambda) v_w^3 \tag{2.1}$$

Tip-speed ratio,

$$\lambda = \frac{R_{blade}\omega_m}{v_w}$$

Where,

ρ_{air} is the density of air, A_{blade} is the area of the blades swept by the rotor [m^2], v_w is the wind speed [m/s], β is called the pitch angle, ω_m is the angular speed of the blades, R_{blade} is the radius of the rotor blades. $C_p(\lambda,\beta)$ is called the 'coefficient of performance' and it is a function of tip speed ratio and the pitch angle. In the operating region of the wind turbine (between the cut-in and cut-out wind speeds), the coefficient of performance is maximum for pitch angle equal to zero. Therefore, throughout the simulation, the pitch angle has been kept constant at 0^o. The wind turbine model in PSCAD calculates the coefficient of performance based on the tip speed ratio at any given wind speed. But when the wind speed increases above the cut-out speed, the pitch angle is changed such that the output power always equals the nominal power [25].

2.2.1 Implementation in PSCAD

PSCAD has two models for wind turbines namely MOD-2 and MOD-5 type. MOD-2 type turbine has been selected for this thesis since it is more suitable for three bladed turbines.

The wind turbine model has inputs for wind speed, angular velocity of the generator and pitch angle, 'β'. There is an inbuilt block known as the 'wind source' in PSCAD that can be used to provide the wind speed input.

The input 'β' is supplied by the wind turbine governor. The block compares the output power of the DFIG with a set reference nominal power that is provided as an input. It has to be noted that the output power to be compared with the reference power should be in per unit with the double fed induction generator rated output as the base. If

the wind speed reaches a limit where the power generated by the DFIG becomes greater than the nominal power the pitch angle changes to a value higher than zero. Under normal wind conditions, the pitch angle is maintained at zero degrees. The wind turbine system built in PSCAD has been shown in figure 2.1 below.

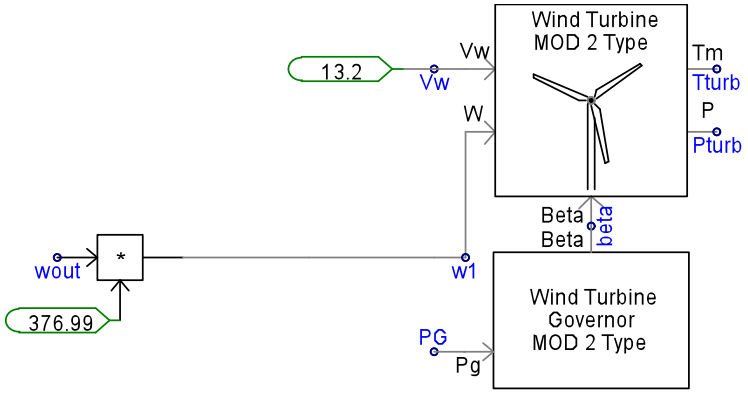

Figure 2.1 Wind turbine, governor and wind source in PSCAD

The wind speed has been set to a value where the generator is generating power close to the nominal power output. Tables 2.1 and 2.2 present the values of various parameters associated with the wind turbine and the wind turbine governor. Table 2.3 represents the wind conditions that have been selected for the simulation.

Table 2.1 Parameters of the wind turbine

Input Parameter	**Value**
Generator rated MVA	1.5 MVA
Machine rated angular mechanical speed	376.99 rad/s or 60Hz
Rotor radius	40 m
Rotor area	5026 m^2
Air density	1.225Kg/m^3
Gear box efficiency	0.979
Gear ratio	90.5
Equation for power coefficient	MOD 2

Table 2.2 Parameters of the wind turbine governor

Input parameter	Value
Variable pitch control	enabled
Type of generator	induction
Turbine rated power	1.5 MW
Reference power output	1.45 MW
Rated electrical frequency	60 Hz
Governor type	MOD 2

Table 2.3 Parameters of the wind source

Input parameter	Value
Mean speed at reference speed	7 m/s
Wind speed input	6.2 m/s

2.3 Wind Generator modeling and control

2.3.1 Doubly Fed Induction machine

The real and reactive power outputs of a grid connected DFIG are dependent on the output phase currents flowing in all the three phases. This makes the control of the real and reactive power dependent on each other and in turn results in poor machine response.

$$P_{out} = \mathrm{Re}(v_a i_a^* + v_b i_b^* + v_c i_c^*) \tag{2.2}$$

$$Q_{out} = \mathrm{Im}(v_a i_a^* + v_b i_b^* + v_c i_c^*) \tag{2.3}$$

Thus, the machine control is carried out in the d-q frame of reference rather than the phase frame of reference.

$$P = \frac{3}{2}(V_d I_d + V_q I_q) \tag{2.4}$$

$$Q = \frac{3}{2}(V_q I_d - V_d I_q) \tag{2.5}$$

Choice of appropriate reference frame results in decoupled control of the real and reactive power output of the DFIG. It can be observed from equations 2.4 and 2.5 that if V_d or V_q becomes zero, then the control of P and Q can be done independently. Decoupled control of real and reactive power output results in better performance of the DFIG.

The transformation of three phase stator and rotor variables to d-q axis variables is achieved in two steps. The first step involves three phase to two phase transformation of both stator and rotor three phase variables along the αβ frame of reference using the Clarke's transform. The second step involves the rotation of the αβ quantities along the arbitrary d-q axis frame of reference that is chosen based on the control requirements.

The power output of a DFIG is the addition of the stator and rotor output powers. The control of these output powers is achieved through appropriate switching of the bidirectional converter system. The rotor side converter controls the real and reactive power exchange between the stator and the grid whereas the grid side converter maintains the DC link voltage at a constant value or in other words controls the real and reactive power exchange between the rotor and the grid.

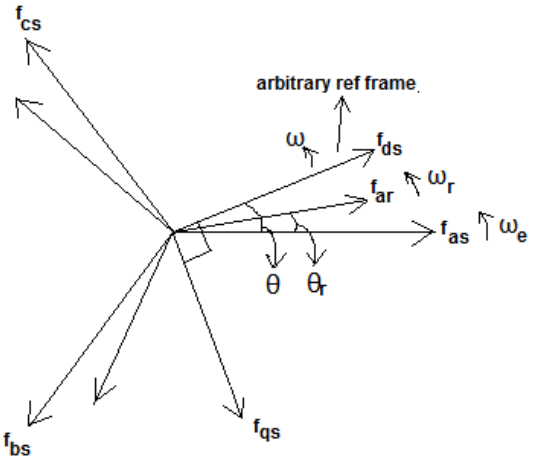

Figure 2.2 abc to dq transformation in case of induction machines [9]

Figure 2.2 aids in developing the d-q axis transformation for a doubly fed induction generator. Both stator and rotor quantities are transformed along the arbitrary frame of reference. This brings both the stator and rotor quantities, originally rotating at different angular speeds, onto a uniform frame of reference in turn making the decoupled control possible to implement.

2.3.1.1 Doubly Fed Induction Generator in PSCAD

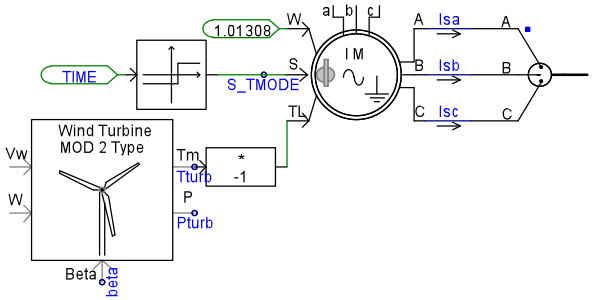

Figure 2.3 DFIG model in PSCAD

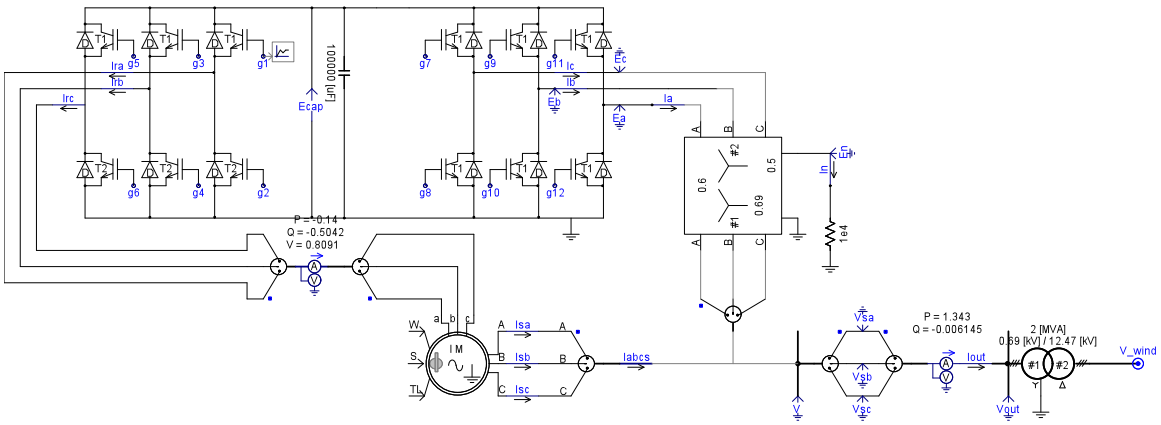

Figure 2.4 Stator and rotor side converters in PSCAD

Figure 2.3 represents the doubly fed induction machine model used in PSCAD as a DFIG. Figure 2.4 shows the bidirectional converter system connected at the rotor end of the machine. The doubly fed induction machine model in PSCAD comprises of inputs for initial machine angular speed (‘W’), machine control mode (‘S’), Input torque (‘TL’). The machine is started in the speed control mode and then switched to torque control mode after some time. The objective of switching the machine to torque control mode is to enable it to generate power based on the existing wind conditions. The significance of the initial machine speed is that an appropriate value can help reducing the machine transients when the machine shifts from speed control to torque control mode. The reason for starting the machine in speed control mode is to speed up the simulation since the machine takes a considerable amount of time to initialize in the torque control mode. Once the machine is initialized, the machine control is shifted from speed control to torque control mode in 0.2 seconds after the start of the simulation. The torque notation is that the doubly fed induction machine is in generation mode when the input torque is

negative. The electrical node 'V_wind' at the rightmost end of figure 2.4 is the point of connection of the grid connected DFIG to the 12.47 kV distribution system described in the appendix A-1. The parameters of the DFIG used in PSCAD have been tabulated in table 2.4.

Table 2.4 Parameters of the Doubly Fed Induction Machine

Input Parameter	**Value**
Rated Power	1.5MVA
Rated Voltage (L-L)	0.69 kV
Angular Frequency	376.99 rad/s
Stator/rotor turns ratio	0.3
Angular moment of inertia	0.85 [s]
Mechanical damping	0.0001 [p.u]
Stator resistance	0.043 [p.u]
Wound rotor resistance	0.0613 [p.u]
Magnetizing inductance	1 [p.u]
Stator leakage inductance	0.0613 [p.u]
Wound rotor leakage inductance	0.0613 [p.u]

2.3.2 Rotor side converter control:

The purpose of the rotor side converter is to control the real and reactive power flowing between the stator and the grid. The real and reactive power transaction between the stator and grid can be expressed as [11]:

$$P_{stator} = \frac{3}{2}(V_{ds}i_{ds} + V_{qs}i_{qs}) \tag{2.6}$$

$$Q_{stator} = \frac{3}{2}(V_{qs}i_{ds} - V_{ds}i_{qs}) \tag{2.7}$$

It is obvious from equations 2.6 and 2.7 that the real and reactive power flows cannot be controlled independently using the d and q axis currents. Thus, the rotor side converter is

controlled in the stator flux oriented reference frame in order to decouple the control of real and reactive power flows associated with the stator. In the stator flux oriented frame,

$$\lambda_{ds} = \lambda_s \tag{2.8}$$

$$\lambda_{qs} = 0 \tag{2.9}$$

If the resistance of the windings is negligible,

$$V_{ds} = 0 \tag{2.10}$$

$$V_{qs} = V_s \tag{2.11}$$

Substituting the above obtained relationships in equations 2.6 and 2.7 gives,

$$P_{stator} = \frac{3}{2} V_{qs} i_{qs} = \frac{3}{2} V_s i_{qs} \tag{2.12}$$

$$Q_{stator} = \frac{3}{2} V_{qs} i_{ds} = \frac{3}{2} V_s i_{ds} \tag{2.13}$$

Since the stator active and reactive powers have to be controlled using the rotor currents, the above relationships have to be modified to include rotor d and q axes currents in the active and reactive power relationships.

The equation for d and q axes flux linkages can be expressed as:

$$\lambda_{ds} = L_s i_{ds} + L_m i_{dr} \tag{2.14}$$

$$\lambda_{qs} = L_s i_{qs} + L_m i_{qr} \tag{2.15}$$

In the stator flux oriented frame, i_{ds} and i_{qs} can be expressed in terms of i_{dr} and i_{qr} respectively as:

$$i_{ds} = \frac{\lambda_{ds} - L_m i_{dr}}{L_s} \tag{2.16}$$

$$i_{qs} = -\frac{L_m}{L_s} i_{qr} \tag{2.17}$$

In the stator flux oriented frame, the d-axis stator flux is constant and equal to λ_s. Therefore, using the relationships obtained in equations 2.16 and 2.17 and applying them to the active and reactive power terms obtained in equations 2.12 and 2.13 gives [11]:

$$P_{stator} = \frac{3}{2} V_s \left[-\frac{L_m}{L_s} i_{qr} \right] = -\frac{3}{2} \frac{L_m}{L_s} V_s i_{qr} \tag{2.18}$$

$$Q_{stator} = \frac{3}{2} V_s \left[\frac{\lambda_s - L_m i_{dr}}{L_s} \right] = \frac{3}{2} \frac{V_s}{L_s} \left[\frac{\lambda_s}{} - L_m i_{dr} \right] \tag{2.19}$$

The above equations establish the relationship between the real and reactive power flows associated with the stator and the rotor d and q axis currents.

According to equations 2.18 and 2.19, the stator real and reactive powers can be controlled solely using the q and d axis components of the rotor current. In other words, PI controllers can be used to generate q and d axis rotor currents based on the error between the reference and the actual stator real and reactive powers. The angular speed of the rotor is used as a measure of the active power exchange between the rotor and the grid. The reference angular speed is based on a fixed tip speed ratio calculated using the initial wind speed and angular speed 'W' (when the machine is in speed control mode). These reference d and q axis currents are in turn used to generate the reference phase currents using the inverse Park's transformation. The reference phase currents generate the switching signals for the rotor side converter using hysteresis controllers. Figure 2.5 shows the speed control loop implemented for rotor side converter control in PSCAD.

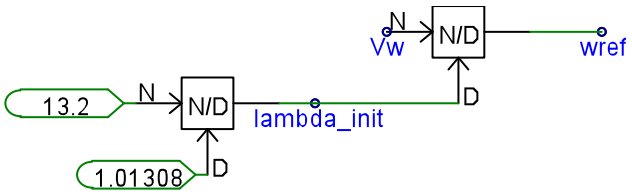

Figure 2.5 Generation of reference angular speed

The main requirement for the rotor side converter control is the determination of the stator flux angle. The procedure for stator flux angle determination is as follows:

$$\frac{d}{dt}\lambda_{\alpha,\beta s} = v_{\alpha,\beta s} - r_s i_{\alpha,\beta s} \tag{2.20}$$

$$\lambda_{\alpha,\beta s} = \int (v_{\alpha,\beta s} - r_s i_{\alpha,\beta s}) dt \tag{2.21}$$

$$\lambda_{s\alpha s} = \sqrt{\lambda_{\beta s}^2 + \lambda^2} \tag{2.22}$$

$$\phi_s = \tan^{-1}\left(\frac{\lambda_{\beta s}}{\lambda_{\alpha s}}\right) \tag{2.23}$$

The implementation of above equations has been carried out in PSCAD and the figures 2.6 and 2.7 represent the block diagram built in PSCAD for the determination of stator flux angle and the reference q axis rotor current respectively.

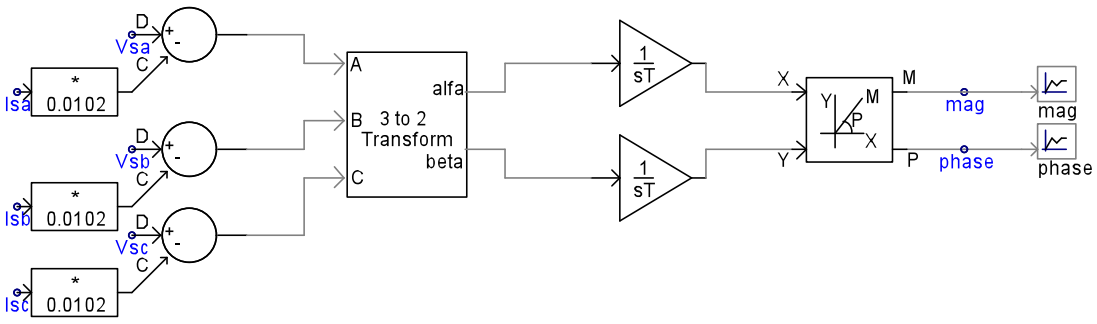

Figure 2.6 Stator flux angle determination [12]

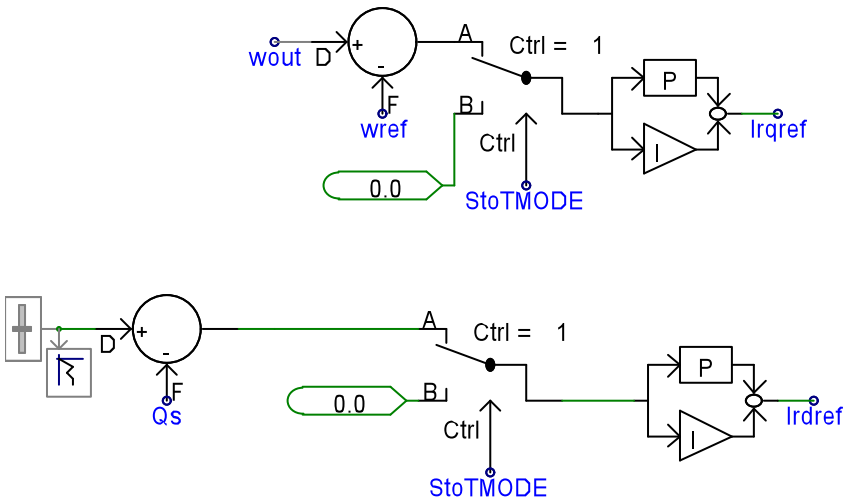

Figure 2.7 Generation of reference d and q rotor currents [12]

The signal "StoTMODE" in figure 2.7 is provided as a control signal to a two input selector. This signal controls the inputs to the two proportional integral controllers meant for stator active and reactive powers. When the machine is operated in the speed control mode, the input to the both the proportional-integral controllers is zero and as soon as the machine is switched to torque control mode, the inputs change from zero to the respective error signals. The parameters chosen for the PI controllers, as shown in figure 2.7, for the

generation of reference q and d axis rotor currents have been shown in tables 2.5 and 2.6 respectively.

Table 2.5 Parameters of the PI controller for generating I_{rqref}

Input Parameter	Value
Proportional gain (K_p)	0.5
Integral time constant (K_p/K_i)	0.1666
Initial output of the integrator	0.2

Table 2.6 Parameters of the PI controller for generating I_{rdref}

Input Parameter	Value
Proportional gain	0.25
Integral time constant	0.1666
Initial output of the integrator	0.075

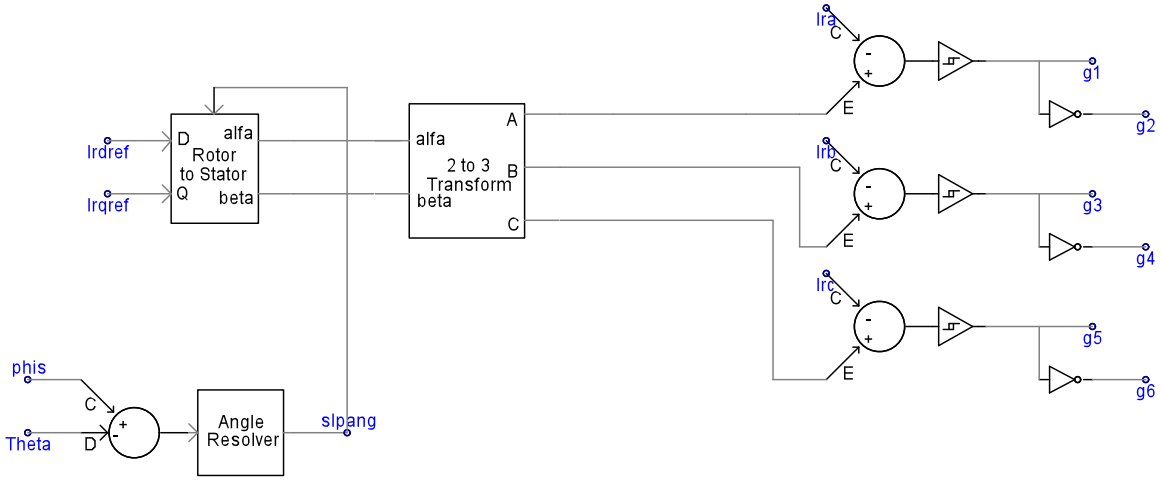

Figure 2.8 Generation of switching signals using hysteresis control [12]

The generation of switching signals using the d and q axis rotor currents is illustrated in the figure above. The implementation of the inverse d-q axis transformation can be interpreted using figure 2.2. In the stator flux oriented frame, the angular speed of the arbitrary reference frame is the same as the stator flux angular speed. The angle 'θ' in figure 2.2 is the stator flux angle (ϕ_s) that is determined using the implementation illustrated in figure 2.6. The rotor angle 'θ_r', as in figure 2.8, at any time instant is determined using a position sensor inbuilt in the doubly fed induction machine model in PSCAD. The angle 'slpang' that is the difference between the stator flux angle and the rotor angle is used to transform the reference rotor currents in d-q axis stator flux oriented frame into three phase currents in the rotor reference frame. The actual three phase rotor currents are made to approximate the reference three phase rotor currents using hysteresis controllers. Hysteresis controllers make sure that the actual phase currents lie within a specified band around the reference phase currents. Table 2.7 has the values for the hysteresis band selected for the controller.

Table 2.7 Hysteresis controller bandwidth in PSCAD

Parameter	**Range**
Hysteresis band	0.005 to -0.005

2.3.3 Grid side converter control

The main purpose of the grid side converter is to keep the DC link voltage constant and decouple the operation of rotor side and grid side converters. In other words, the grid side converter controls the active and reactive power exchange between the rotor and the

grid. Decoupled control of real and reactive power flow is achieved using the supply side voltage oriented frame. In the supply side voltage oriented frame,

$$V_d = V_s \tag{2.24}$$

$$V_q = 0 \tag{2.25}$$

Therefore, the power flow equations become,

$$P_r = \frac{3}{2}(V_d i_d) \tag{2.26}$$

$$Q_r = -\frac{3}{2}(V_d i_q) \tag{2.27}$$

Thus the real power can be controlled using the d-axis component of the current flowing between the grid side converter and the grid. Similarly, the reactive power can be controlled using the q-axis component of the current flowing between the grid side converter and the grid.

The most significant part of the control scheme implementation is the determination of the supply side voltage angle determination. The supply side voltage angle is determined as shown in figure 2.9.

$$\phi_{V_s} = \tan^{-1}\left(\frac{V_\beta}{V_\alpha}\right) \tag{2.28}$$

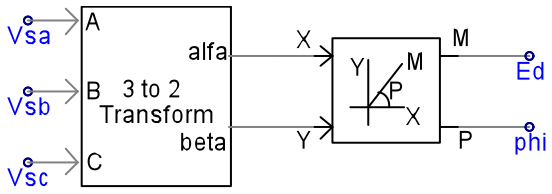

Figure 2.9 Supply side voltage angle determination in PSCAD [12]

After obtaining the stator voltage angle, the three phase currents flowing between the grid side converter and the grid are transformed to the supply side voltage oriented frame using the supply voltage angle. The block diagram in PSCAD has been shown in figure 2.10.

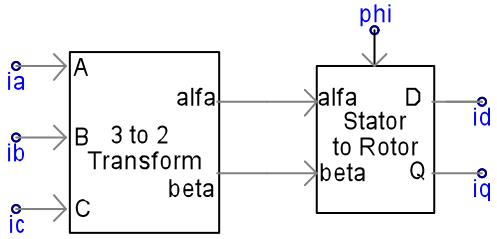

Figure 2.10 abc to dq conversion of currents

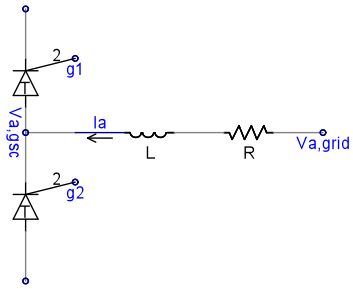

Figure 2.11 Circuit associated with grid side converter (phase 'a')

The mathematical equations defining the relationship between the d-q axis voltages on the grid side and the terminals of the grid side converter, as shown in figure 2.11, in the supply side voltage oriented frame are given as [11]:

$$v_{d,grid} = R i_d + L \frac{di_d}{dt} - \omega L i_q + v_{d,gsc} \tag{2.29}$$

$$v_{q,grid} = R i_q + L \frac{di_q}{dt} + \omega L i_d + v_{q,gsc} \tag{2.30}$$

The switching signals to be provided to the switches of the grid side converter are controlled by the d and q axis components of the grid side converter voltage. The grid side converter voltage is in turn dependent on the d and q axis components of the current flowing between the grid and the converter. Thus, the d and q axis current components control the converter side voltage that operates the converter switches and in turn control the real and reactive power exchange between the rotor and the grid. It is visible from equations 2.29 and 2.30 that $v_{d,gsc}$ and $v_{q,gsc}$ are dependent on both i_d and i_q. This makes the equations coupled and the control complex. To decouple the equations, dummy variables $v'_{d,grid}$ and $v'_{q,grid}$ are introduced and defined as [11]:

$$v^*_{d,gsc} = -\omega L i_q + v'_{d,grid} \tag{2.31}$$

$$v^*_{q,gsc} = \omega L i_d - v'_{q,grid} \tag{2.32}$$

Where, $v^*_{d,grid}$ and $v^*_{q,grid}$ are the reference d and q axis grid side converter voltages.

The substitution of reference d and q axis grid side converter side voltages obtained in the above equations in equations 2.29 and 2.30 gives:

$$v'_{d,grid} = Ri_d + L\frac{di_d}{dt} \tag{2.33}$$

$$v'_{q,grid} = Ri_q + L\frac{di_q}{dt} \tag{2.34}$$

Thus, PI controllers are used to reflect the error in i_d on $v'_{d,grid}$ and i_q on $v'_{q,grid}$ respectively. In PSCAD, the control system is built as shown in figure 2.12.

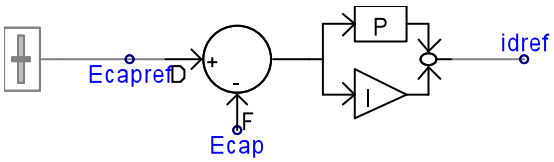

Figure 2.12 Generation of i_{dref} based on the error in capacitor voltage

The parameters of the PI controller used for obtaining the reference d-axis current for the grid side converter have been presented in table 2.8.

Table 2.8 Parameters of the PI controller for capacitor voltage

Input parameter	**Value**
Reference capacitor voltage, Ecapref	0.8 kV
Proportional gain, K_p	5
Integral time constant, T_i	0.01
Initial output of integrator	0

The implementation of equations 2.31-2.34 in PSCAD to obtain the reference d-axis grid side converter voltage has been shown in figure 2.13.

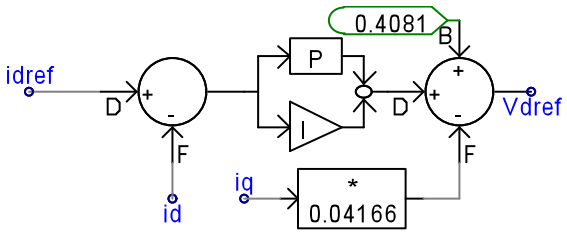

Figure 2.13 Generation of d-axis reference grid side converter voltage [12]

The parameters of the PI controller used in figure 2.13 for the generation of '$V_{d,grid}$'' have been shown in table 2.9.

Table 2.9 parameters of the PI controller for generating $v'_{d,grid}$

Input parameter	Value
Proportional gain, K_p	10
Integral time constant, T_i	0.01
Initial output of integrator	0

$V_{d,grid}$ is the peak value of the voltage at the secondary side of the 0.69/0.5 kV transformer.

$$v_{d,grid} = \frac{\sqrt{2}}{\sqrt{3}}(0.5)\text{kV} = 0.4081\text{kV}$$

The inductance of the circuit in figure 2.11 is the leakage reactance of the 0.69/0.5 kV transformer.

$$Z_{base} = \frac{0.5^2}{0.6}\Omega = 0.4166$$

$$X_{leakage,transformer,p.u} = 0.1\text{p.u}$$

$$X_{leakage,transformer,\Omega} = 0.04166$$

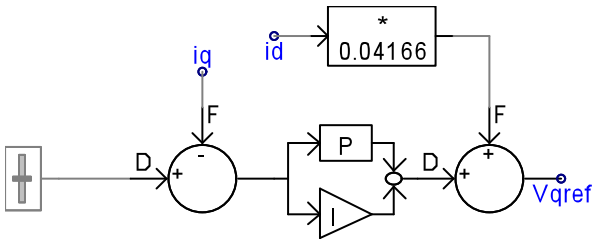

Figure 2.14 Generation of q-axis reference grid side converter voltage [12]

The reference value selected for $i_{1q,ref}$ is zero since the wind generator is made to operate at a power factor close to unity. The parameters of the PI controller used in figure 2.14 for the generation of '$V_{q,grid}$' have been shown in table 2.10.

Table 2.10 Parameters of the PI controller for generating $v'_{q,grid}$

Input parameter	Value
Proportional gain, K_p	10
Integral time constant, T_i	0.01
Initial output of integrator	0

The generation of reference d and q axis converter end voltages is followed by converting these voltages to phase frame of reference and it has been shown in figure 2.15.

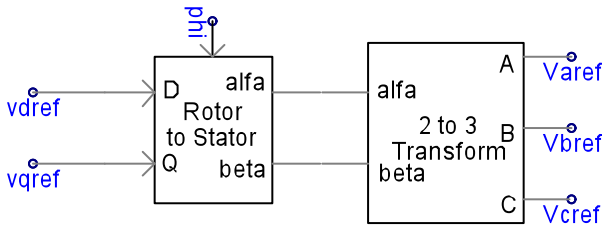

Figure 2.15 Conversion of reference voltages from d-q to phase frame

The gating signals are generated by using the above obtained reference voltage signals and applying them to a sinusoidal pulse width modulator (PWM) [12]. The implementation of the technique in PSCAD has been shown in figure 2.16.

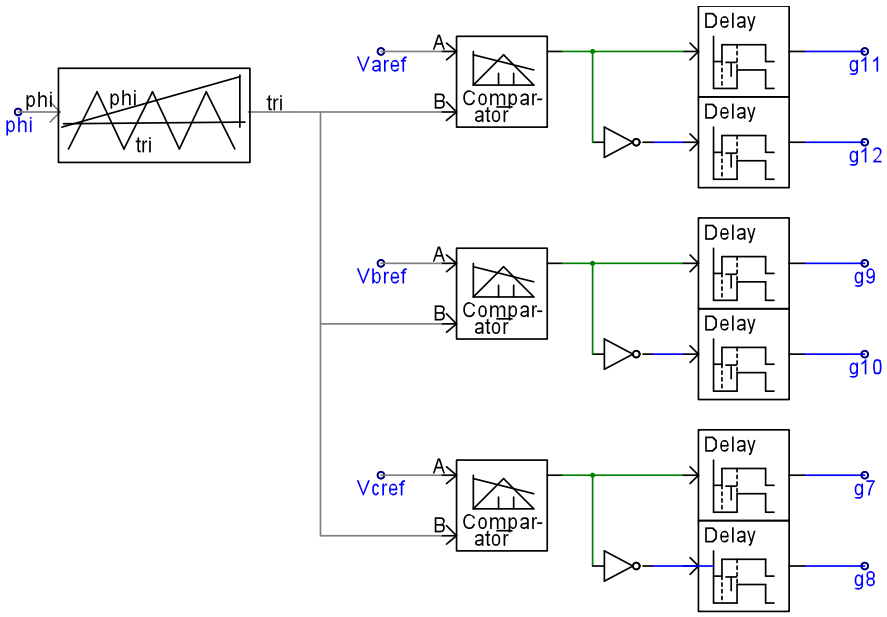

Figure 2.16 Generation of gating signals for grid side converter [12]

2.4 Steady state results

It is very necessary to confirm the steady state performance of the grid connected DFIG in the distribution system. Any inappropriate results such as oscillations in real or reactive power result in continuously varying voltages or bus angles at the buses in the system. Incorporation of such a model for fault studies would result in incorrect results. In other words, proper steady state operation of the DFIG ensures correct implementaion of the control scheme.

The real and reactive power outputs of the DFIG have been presented in the plots shown in the figures below. The figure 2.17 shows the current supplied by the DFIG. The output current is directly related to the real power output of the machine, shown in figure 2.18, given that the voltage at the terminal of the DFIG is stable. The figure 2.19 shows

the voltage at the terminal of the DFIG. Similar to the current, the voltage at the terminal and throughout the distribution system is directly related to the reactive power output of the machine , shown in figure 2.20. An oscilatory reactive power output would result in fluctuating voltages in the system. The machine having fluctuating voltages at its terminals, in turn, cannot be integrated to the distribution system and used for fault studies since it would result in incorrect results. Therefore, it is absolutely essential to make sure that the machine has a good steady state performance before proceeding to fault studies. The ramp up time of the real and reactive powers can be observed to be different and is dependent on the gain settings for the PI controllers used for controlling the real and reactive powers. There is a sudden change in the real and reactive power outputs at t=0.2 seconds because of the switching of the machine control from speed control mode to torque control mode.

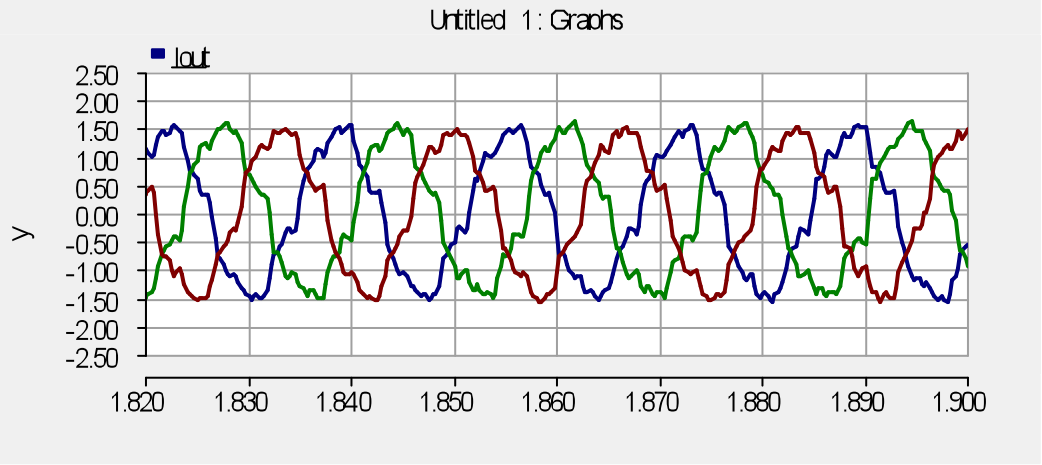

Figure 2.17 Output current out of the wind generator

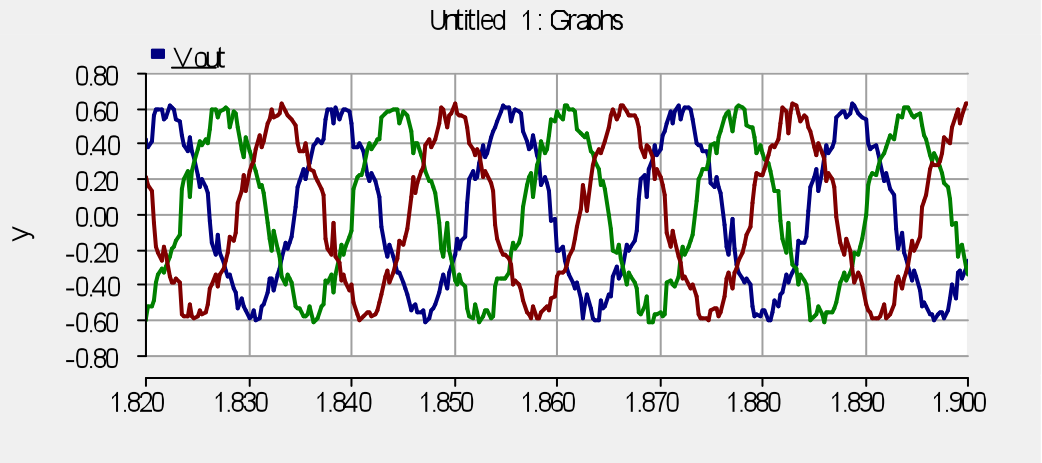

Figure 2.18 Output voltage at the terminal of the wind generator

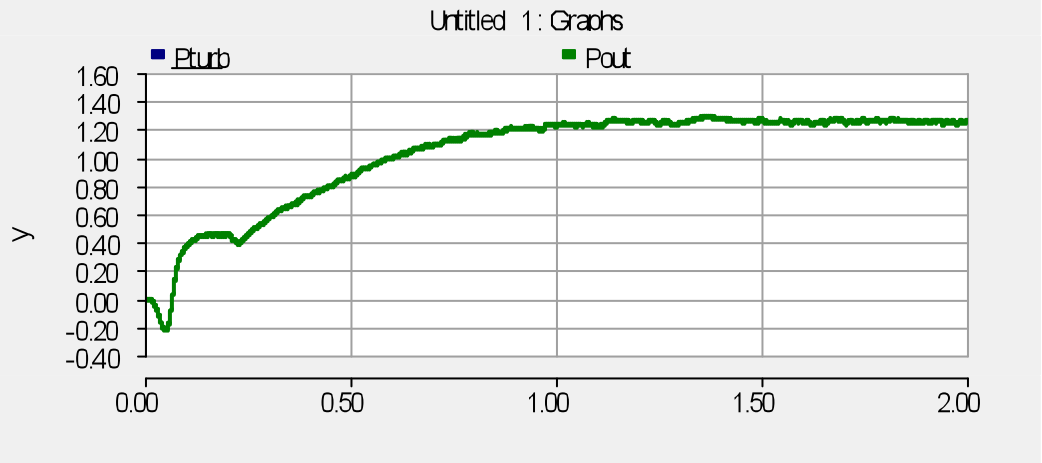

Figure 2.19 Output active power of the wind generator (in MW)

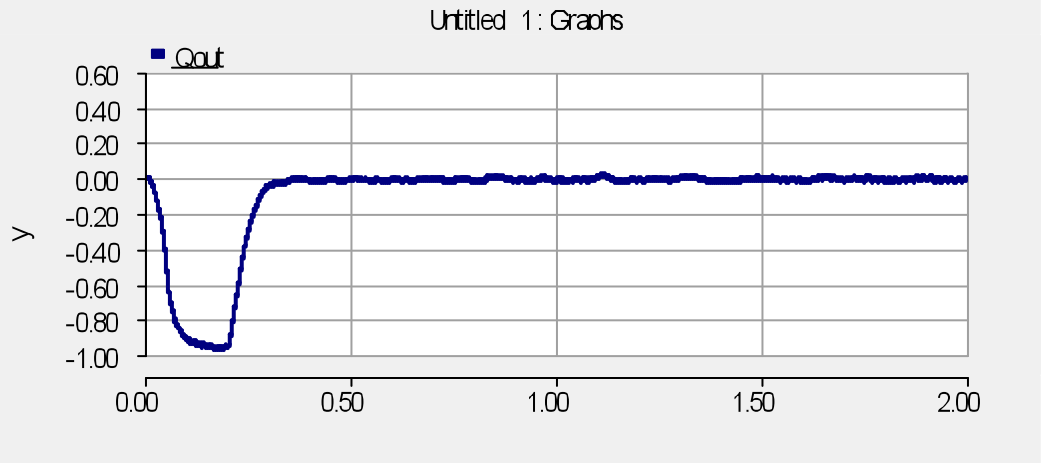

Figure 2.20 Output reactive power of the wind generator (in MVAr)

CHAPTER 3

GRID CONNECTED PHOTOVOLTAIC GENERATION: CONTROL AND IMPLEMENTATION IN PSCAD

3.1 Introduction

This chapter covers the implementation of the control scheme of a three phase grid connected photovoltaic generator. The photovoltaic generation in PSCAD is designed to generate 0.6 MW of power. The entire model consists of a solar array, a M.P.P.T controller, d.c link capacitor, a three phase inverter and a terminal node (connected to a certain bus in the distribution system). The model has two solar arrays connected in parallel. Each array produces 0.3 MW of power. The PV array in PSCAD is a custom built model that produces d.c voltage based on the amount of solar insolation and cell temperature. Each of the arrays is made to operate at its maximum power point. PSCAD has a custom built model for maximum power point tracking that uses the voltage and current values ('V_{pv}' and 'I_{pv}') out of the array and determines the maximum power point for any existing condition. A d.c-d.c converter is used to make the array operate at its maximum power point voltage [19]. A three phase inverter maintains the voltage across the d.c link capacitor to be constant and in turn controls the active and reactive power flow between the panel and the grid.

3.2 PV array

The PV array, used for building the grid connected system, is an inbuilt block in PSCAD that uses the solar insolation and cell tempertaure, as inputs, to compute the amount of power generated by the array.

As mentioned in the introduction, the current equation for a PV cell is given as:

$$I = I_{sc} - I_o\left[\exp\left(\frac{V + IR_{sr}}{nkT_c / q}\right) - 1\right] - \left(\frac{V + IR_{sr}}{R_{sh}}\right)$$

All the parameters governing I_{sc} and I_o, except the solar insolation and cell temperature, are fed as fixed inputs to the block. The cell tempertaure,T_c and the solar insolation,G are available as variable inputs to the block. The block calculates the output current and d.c voltage of the array based on the arrangement of solar cells in the array. The details of the organization of the cells in the array is also fed as a fixed input to the block. The PV array block in PSCAD has been shown below in figure 3.1.

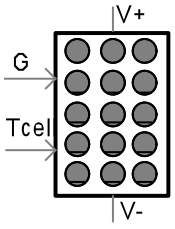

Figure 3.1 PV array block in PSCAD

The I-V curve of the solar array is used to determine the maximum power point voltage that is required for ensuring the optimum operation of the solar array. The values chosen for various parameters in the simulation have been listed in table 3.1.

Table 3.1 Parameters of solar array

Input parameter	**Value**
Solar radiation	607.407 W/m^2
Cell temperature	50^{o}C
d.c link capacitor	0.8 kV
Number of modules in series	20
Number of module strings in parallel	20
Number of cells connected in series	108
Number of cell strings in parallel	7
Reference irradiation	1000
Reference cell temperature	25
Effective area/cell	0.01m^2
Series resistance/cell	0.02 Ω
Shunt resistance/cell	1000 Ω
Diode ideality factor	1.5
Band gap energy	1.103 eV
Short circuit current at ref. conditions/cell	2.5 A
Temperature coefficient of photocurrent	0.001

3.3 Maximum power point tracking (MPPT)

The maximum power point tracking is achieved in PSCAD using an inbuilt MPPT block. The block calculates the value of the maximum power point voltage using the output current, I_{pv} and output voltage, V_{pv}. It is important to note that the maximum power point voltage always corresponds to maximum power point. In other words, the maximum power point voltage under any amount of solar insolation and cell temperature

is the same for any other values of solar insolation and cell temperature. The only thing that changes with the change of the existing solar conditions is the array output current.

A dc-dc converter is used for the purpose of achieving the maximum power point tracking [19]. Once the value of the maximum power point voltage is known, it is compared to the actual dc voltage across the capacitor, C1 or V_{pv}. The error signal is passed through a PI controller that generates the switching signal for the d.c-d.c converter. It is very important to note that the PV array is a current source. The figure 3.2 shows the dc-dc converter used for maintaining the voltage across the capacitor, C1 to be equal to maximum power point voltage. Since the switching signal for the d.c-d.c converter has to be square shaped, a comparator is used to generate the square waves based on the comparison of the output signal out of the PI controller and a reference traingular wave, as shown in figure 3.3. The values of the gains set for the above mentioned PI controller have been given in table 3.2.

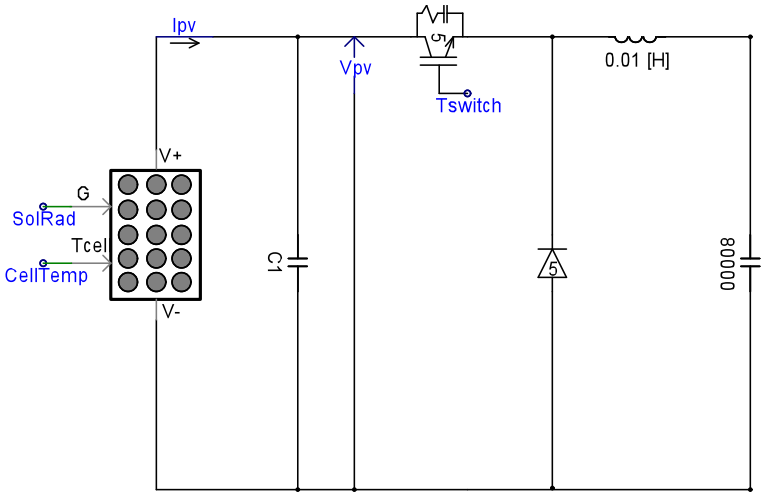

Figure 3.2 dc-dc converter for tracking the MPP voltage [19]

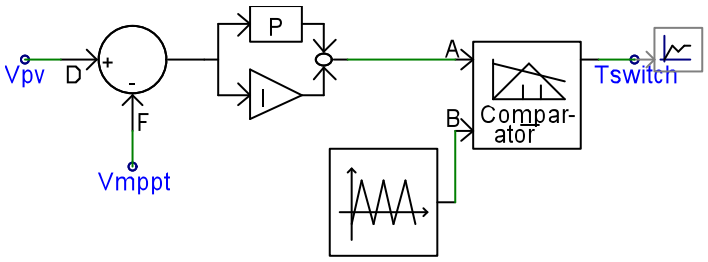

Figure 3.3 Generation of switching signal 'Tswitch' for dc-dc converter [19]

Table 3.2 Parameters of the PI controller used for generation of 'Tswitch'

Input parameter	**Value**
Proportional gain, K_p	0.4
Integral time constant, T_i	0.5
Initial output of integrator	0.9

3.4 Three phase inverter

A three phase inverter is used to connect the photovoltaic array to the grid through a d.c link capacitor. The purpose of the d.c link capacitor is very similar to its functionality in the grid connected DFIG ,i.e., decouple the operation of the dc side and ac side oepration. The three phase converter controls the real and reactive power exchange between the array and the grid. The type of control implemented for the inverter is the simple P and Q control [19]. The implementation of the control scheme results in the generation of the gating signals for the three phase inverter. The three phase inverter used for connecting the array to the grid has been shown in figure 3.4 below.

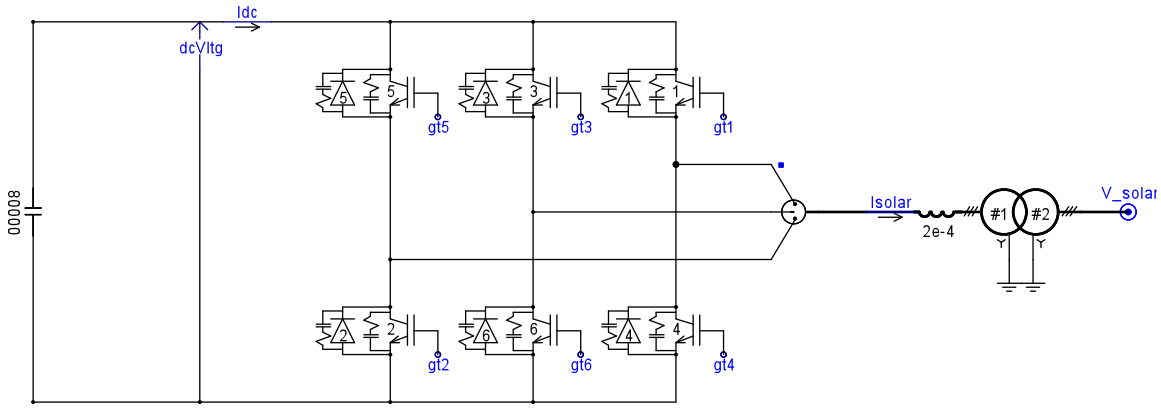

Figure 3.4 Three phase grid side inverter [19]

The inverter is coupled to the grid through a 023/12.47 kV Y-Y transformer. The node 'V_solar' represents the bus at which the photovoltaic generator is connected to the distribution system. It is important to note that figures 3.2 and 3.4 show only one of the two systems connected in parallel. Therefore, the power injected into the grid is twice as much as generated by one system.

3.5 Inverter control

In the simple P and Q control [19], a PI controller is used to generate the angle of the modulating signal that makes the d.c link voltage follow the reference voltage. Similarly, another PI controller generates the magnitude of the modulating signal that makes the reactive power exchange between the grid and the PV generator to be equal to the reference value. The reference reactive power has been selected to be zero as the PV power generator has been operated at a power factor close to unity. Figure 3.4 shows the

generation of the angle ('Ang') and the magnitude ('Mag') of the modulating signal using the d.c link voltage and the reactive power respectively.

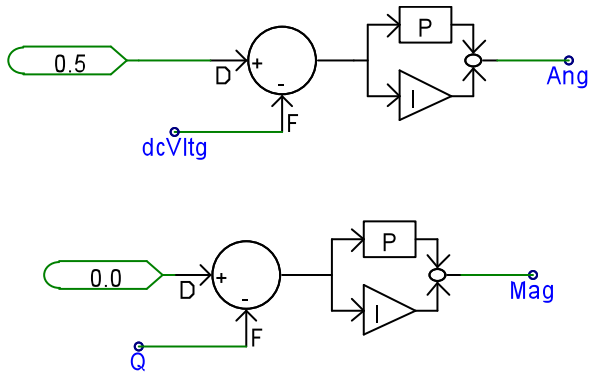

Figure 3.5 Determination of the angle and magnitude of the modulating signal

Table 3.3 Parameters of the PI controller for the generation of 'Ang'

Input parameter	**Value**
Proportional gain, K_p	1
Integral time constant, T_i	0.2
Initial output of integrator	0.75

Table 3.4 Parameters of the PI controller for the generation of 'Mag'

Input parameter	**Value**
Proportional gain, K_p	1
Integral time constant, T_i	0.2
Initial output of integrator	0.75

Tables 3.3 and 3.4 show the values of the parameters of the PI controllers used for the generation of 'Ang' and 'Mag' respectively. The determination of the angle and

magnitude of the modulating signals is followed by the generation of the modulating signals for all the three phases. The modulating signal for each phase is in turn used to generate the gating pulses for inverter leg associated with the phase. Figure 3.5 shows the block diagram in PSCAD used for the generation of gating signals for the inverter.

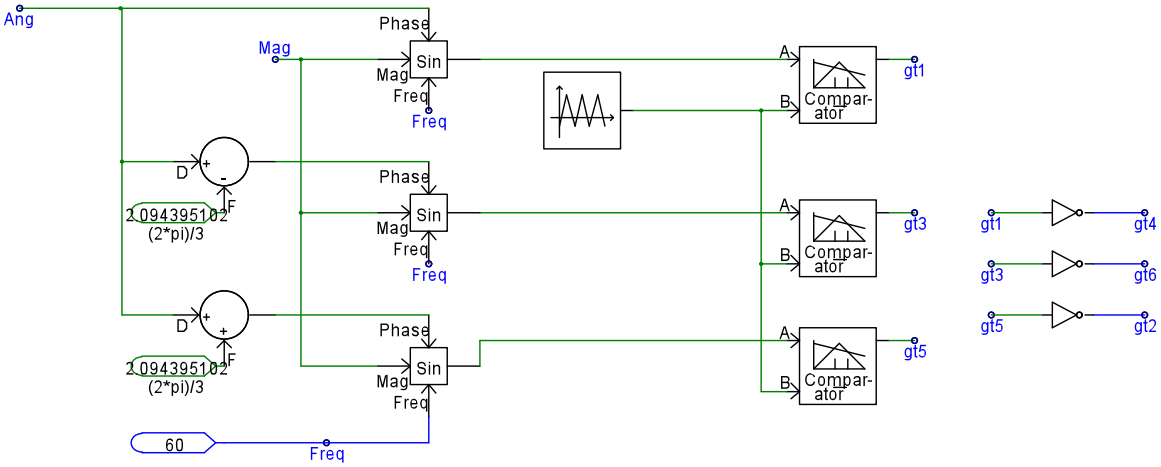

Figure 3.6 Switching signals for the three phase inverter

3.6 Steady state results

Similar to the case of the grid connected DFIG explained in the previous chapter, confirmation of a proper steady state response is necessary before proceeding on to the fault analysis in the distribution system with integrated photovoltaic generation. Conditions such as oscillatory waveform for real or reactive powers resulting due to poorly set PI controllers, offset in values of the parameters as against their reference values due to incorrect implementation of control etc. make the system inappropriate for being used in fault analysis. Therefore, stable and expected steady state results confirm

correct implementation of control scheme for the system. The current supplied by the photovoltaic generator has been shown in figure 3.7. Steady output current cofirms a constant power being supplied by the photovoltaic generator given that the voltage is constant. Figure 3.8 shows the voltage at the terminal of the grid connected photovoltaic system steady at rms value of 7.2kV and it is directly related to the reactive power supplied by the DFIG. Similar to the DFIG, steady output voltage and current are very necessary for making sure that the model is appropriate for being integrated to the distribution system and being used for the fault studies. Figure 3.9 shows the output real power of the machine to be equal to 0.6 MW. Similarly, figure 3.10 confirms the reactive power supplied by the machine to be 0 MVAr and thus the figures approve the correct implementation of control scheme for the grid connected photovoltaic system.

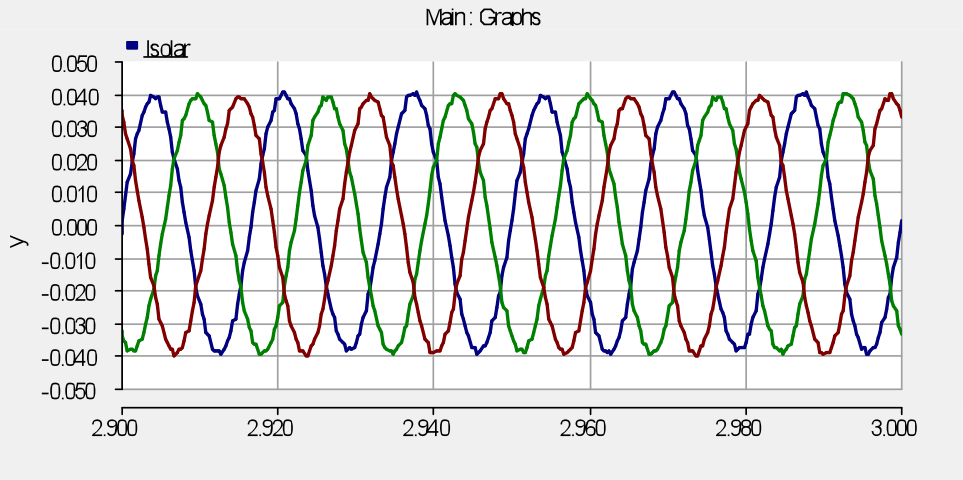

Figure 3.7 Output current from the PV system

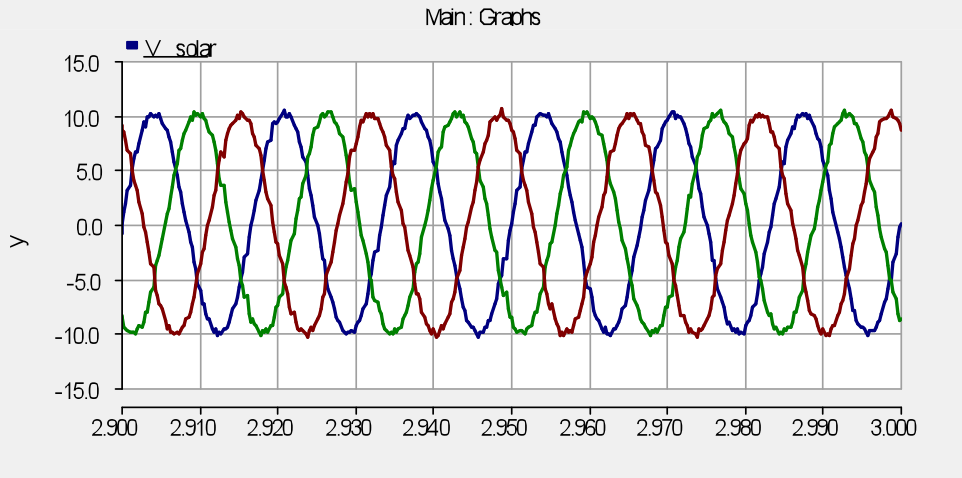

Figure 3.8 Voltage at the terminal of the PV system

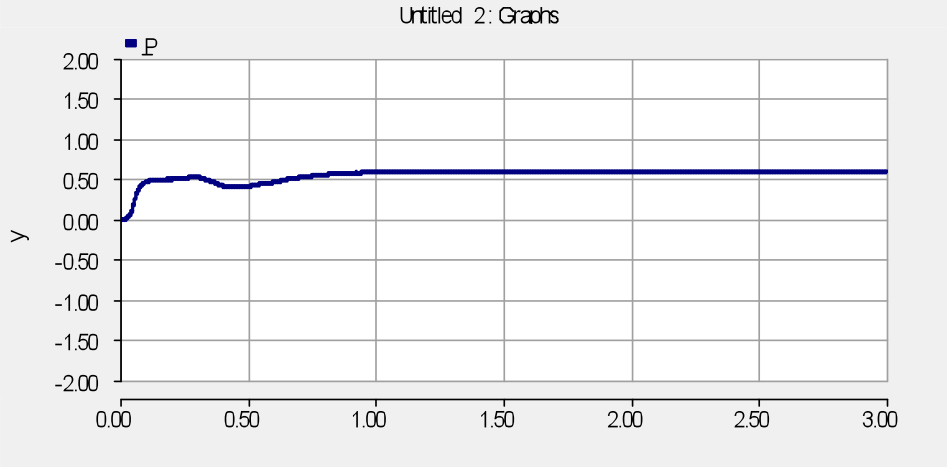

Figure 3.9 Output real power of the PV system (in MW)

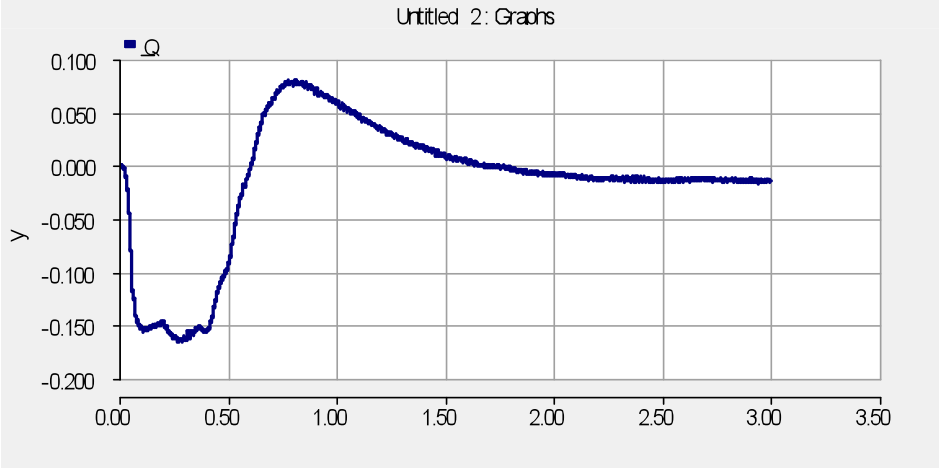

Figure 3.10 Output reactive power of the PV system (in MVAr)

CHAPTER 4

STEADY STATE FAULT ANALYSIS IN UNBALANCED DISTRIBUTION SYSTEMS

4.1 Introduction

The purpose of the thesis is to study the impact of unbalance in the distribution system on the magnitude of fault currents supplied by distributed generators in a 14 bus, 12.47 kV distribution system. The addition of distributed sources, modeled as described in previous chapters, makes the system non-radial. The modeling of various components of the distribution system such as feeders, loads etc. have an effect on the steady state and fault behavior of the system. Although distribution systems have issues of unbalance associated with them; the proximity of distributed generation locations to the distribution systems sometimes makes the integration favorable. The main reason for keeping the reactive power output of the distributed sources to be zero is to prevent any sort of effect on the voltages of the system.

The location of distributed generators is very crucial in relation to the behavior of the system. The renewable sources have been connected at the far-end buses in the system. The primary reason for connecting renewable sources far away from the infinite bus is to make sure that they supply considerable magnitude of currents in event of faults. If the renewable energy sources are installed close to the infinite bus, then for faults anywhere in the system, infinite bus supplies majority of the current. This leads to very small contribution from distributed generators and in turn makes the effect of unbalance on the

operation of distributed generators unclear. The voltage rating of the distribution system and the transformer used to connect the distributed sources to the grid play an important role in their behavior. Most commonly used photovoltaic systems operate at 230V and similarly doubly-fed induction generators are rated at 690V. A high voltage distribution system can result in negligible impact on voltages at the terminal of the distributed generators even though the unbalance on the grid side may be considerable. Also, the type of transformer used to connect the distributed source to the grid plays an important role in the behavior of the distributed source during faults. A star delta transformer has been used to connect the DFIG to the grid that makes the unbalance on the grid side negligible on the terminals of the DFIG. The entire details of the system studied in this thesis are given in the appendix.

4.2 Balanced and unbalanced systems

In order to study the impact of unbalance on the fault current contribution from distributed sources, unbalance has to be created in the system. To achieve this, two cases have been built and simulated in PSCAD. The balanced system involves transposed feeders as well as balanced three phase loads whereas the unbalanced system involves un-transposed feeders and unbalanced loads in each phase. The percentage of unbalance in the system follows the percentage of voltage regulation limits. The transposition of the feeders in the balanced case makes the mutual coupling (explained in the next section) between the lines equal. The loading scheme for the balanced and the unbalanced cases are given as:

Case 1: Balanced loading:

$$\text{Load}_{\text{ph,a}} = \text{Load}_{\text{ph,b}} = \text{Load}_{\text{ph,c}}$$
$$\text{Load}_{\text{ph,a}} + \text{Load}_{\text{ph,b}} + \text{Load}_{\text{ph,c}} = \text{Load}_{3\phi}$$

Case 2: Unbalanced loading:

All the buses except '180' and '200' have loading scheme as under:

$$\text{Load}_{\text{ph,a}} = \text{Load}_{\text{ph,c}}$$
$$\text{Load}_{\text{ph,b}} = 0.3 * \text{Load}_{\text{ph,a}} = 0.3 * \text{Load}_{\text{ph,c}}$$
$$\text{Load}_{\text{ph,a}} + \text{Load}_{\text{ph,b}} + \text{Load}_{\text{ph,c}} = \text{Load}_{3\phi}$$

At buses '180' and '200',

$$\text{Load}_{\text{ph,a}} = \text{Load}_{3\phi}$$

4.3 Load model

It is to be noted that the static constant impedance loads have been used in the simulation [26]. The dependency of loads on the voltage and frequency at the bus is given as:

$$P = P_0 \left(\frac{V}{V_0}\right)^a (1 + K_{Pf} \Delta f)$$
$$Q = Q_o \left(\frac{V}{V_0}\right)^b (1 + K_{Qf} \Delta f)$$

The quantities with subscript '0' refer to the initial operating states of the corresponding quantities. The exponents 'a' and 'b' determine the type of loads. Both of them being 0, 1 or 2 represents constant power, constant current or constant impedance loads

respectively. PSCAD has entries for ‘dP/dV’ and ‘dQ/dV’ of a load at each bus. Using the equations, it can be observed that the quantities are approximately equal to ‘a’ and ‘b’ respectively. Therefore ‘a’ and ‘b’ are measures of sensitivity of real and reactive powers of the load to the voltage at the bus. Similarly, K_{Pf} and K_{Qf} are the measure of sensitivity of real and reactive powers at a load to the frequency at the bus. Constant impedance loads have been used for the simulation with their frequency dependency maintained at zero.

4.4 Feeder model

PSCAD uses travelling wave based method to compute the three phase impedance matrix of each feeder section [27]. The travelling wave based method is the most accurate time domain model for transmission lines, especially for cases where transient phenomena have to be studied such as faults. The approximation of transmission line models using constant frequency representation results in false amplification of magnitudes during faults and thus incorrect values, especially for unbalanced systems. The line equations are solved by PSCAD in frequency domain and then transformed in time domain using the convolution integral. It should be noted that in PSCAD, the time step chosen for simulations should be lower than the travelling time of the wave in the smallest feeder in the network. The feeders connecting the wind and solar generation have been selected to be longer than the rest of the feeders in the system since in actual wind and solar generating stations are located at some distance from the feeders.

4.5 Steady state results

The simulation results for the steady state voltages at all the buses in the balanced and unbalanced system with distributed generation in the system are given in tables 4.1 and 4.2 respectively.

Table 4.1 Steady state voltages in the balanced system (p.u)

Bus number	Voltage (p.u)
0	0.995
20	0.985
40	0.976
50	0.972
100	0.97
110	0.97
60	0.969
140	0.968
160	0.968
70	0.984
80	0.984
180	0.987
200	0.988

Table 4.2 Steady state voltages in the unbalanced system (p.u)

Bus number	Phase 'a' voltage	Phase 'b' voltage	Phase 'c' voltage
0	0.993	0.9973	0.995
20	0.975	1.005	0.976
40	0.964	1.008	0.958
50	0.959	1.009	0.950
100	0.963	1.008	0.957
110	0.964	1.008	0.957
60	0.955	1.010	0.943
140	0.954	1.010	0.941
160	0.955	1.010	0.942
70	0.967	1.011	0.975
80	0.96	1.019	0.977
180	0.955	1.028	0.984
200	0.955	1.03	0.987

It can be observed from the above tables that all the voltages in the system in both the balanced and unbalanced case are within the six percent voltage regulation limits.

4.6 Fault simulation

The main objective of this thesis is to study the impact of unbalance in a distribution system with distributed generation on the magnitude of fault currents in the system. The fault analysis of a system has direct implications on the settings of protective equipment in the system. The DFIG being a dynamic source (induction machine) and the PV system being a static source may introduce a different behavior during faults than conventional synchronous sources. In other words, their impact on fault current magnitudes is expected to be different than conventional synchronous machines of similar power rating. Moreover, the presence of power electronic interface between the distributed generators and the grid causes the behavior to be even more complex. The unbalance in distribution systems has been shown to have an effect on the magnitude of fault currents in the system. Therefore, the results presented in this section show the impact of unbalance in distribution systems the fault currents supplied by the DFIG and PV source. The fault analysis carried out involves the results for faults applied at two different buses (180 and 200) in the system. All types of asymmetrical faults have been studied and the fault currents supplied by wind and solar generators have been presented for both the balanced and the unbalanced system.

4.6.1 Single line to ground fault

The fault currents supplied by the DFIG and photovoltaic system have been presented for a single line to ground fault on phase 'a'. The type of fault has been applied at t=2.58s at the zero crossing of the voltage of phase 'a' at bus 180. Figure 4.1 shows the fault currents supplied by the DFIG and the PV system for the fault at bus 180 in the balanced system. It should be noted that the behavior of the distributed generators is the same in both the balanced and the unbalanced system. Only the magnitude of the peak of fault current differs in the two cases. The color codes for the plots presented are blue for phase 'a', green for phase 'b' and maroon for phase 'c'.

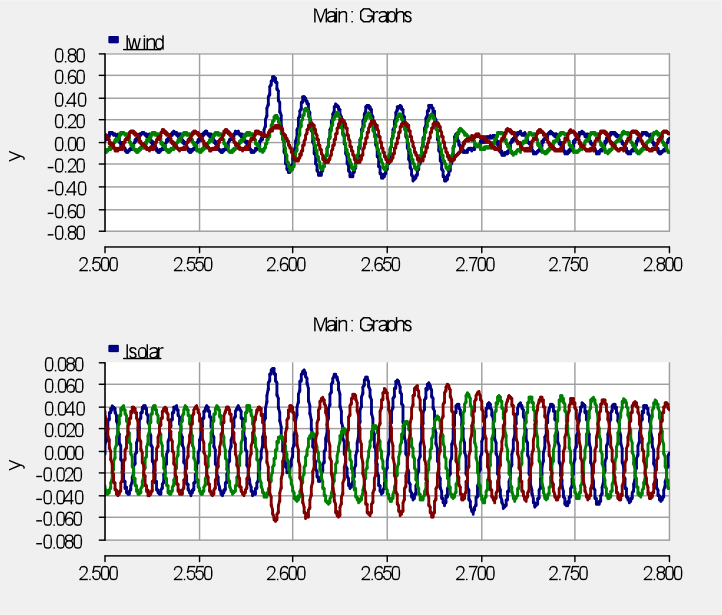

Figure 4.1 Fault current supplied by DFIG and the PV system during the Single line to ground fault at bus 180

The magnitude of peak of fault current supplied by the DFIG and the PV system for a single line to ground fault on phase ‘a’ at buses 180 and 200 have been compared and tabulated for the balanced and unbalanced cases in tables 4.3 and 4.4 respectively.

Table 4.3 Comparison of fault currents supplied by wind and PV generators for single line to ground fault on phase ‘a’ at bus 180

Type of source	Peak fault current (A)		% error
	Balanced system	Un-balanced system	
Wind	583.91	610.284	4.516%
Solar	73.76	73.88	≈0%

Table 4.4 Comparison of fault currents supplied by wind and PV generators for single line to ground fault on phase ‘a’ at bus 200

Type of source	Peak fault current (A)		% error
	Balanced system	Un-balanced system	
Wind	619.814	641.651	3.52%
Solar	68.233	66.73	2.20%

4.6.2 Double line to ground fault

The double line to ground fault has been applied between phases ‘a’ and ‘b’ and ‘a’ and ‘c’ at two different buses 180 and 200 and magnitude of peak fault currents supplied

by the DFIG and the photovoltaic system have been compared. Figure 4.2 depicts the current supplied by the two sources for double line to ground fault between phases 'a' and 'b' at bus 180 in the balanced system. It should be noted that the fault has been applied at the zero crossing of the voltage V_{ab} and V_{ac} at buses 180 and 200 respectively.

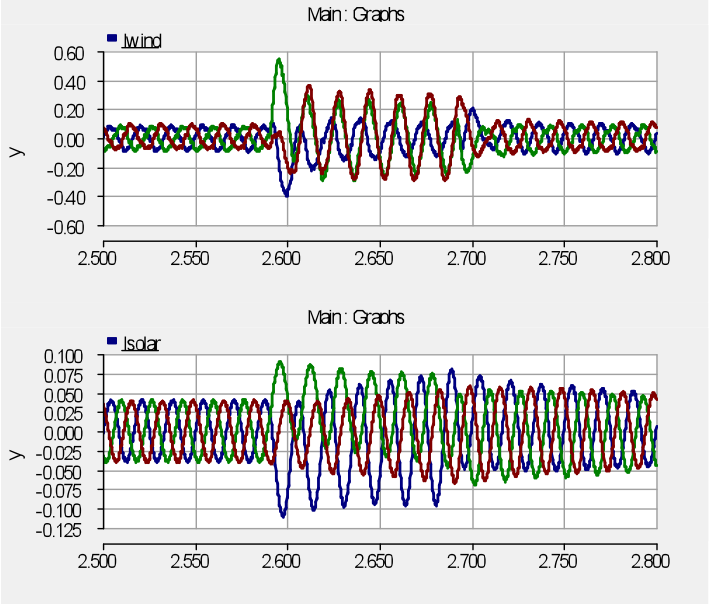

Figure 4.2 Fault current supplied by DFIG and the PV system during the double line to ground fault at bus 180

The magnitude of peak fault currents for double line to ground faults between phases 'a' and 'b' and phases 'a' and 'c' at buses 180 and 200 have been presented in tables 4.5, 4.6, 4.7 and 4.8 respectively.

Table 4.5 Comparison of fault currents supplied by wind and PV generators for double line to ground fault between phases ‘a’ and ‘b’ at bus 180

Type of source	Faulted phase/s	Peak fault current (A)		% error
		Balanced system	Un-balanced system	
Wind	‘a’	400	413.58	3.395
	‘b’	541.343	563.52	4.097
Solar	‘a’	109.62	108.74	0.8%
	‘b’	89.67	88.96	0.79%

Table 4.6 Comparison of fault currents supplied by wind and PV generators for double line to ground fault between phases ‘a’ and ‘b’ at bus 200

Type of source	Faulted phase/s	Peak fault current (A)		% error
		Balanced system	Un-balanced system	
Wind	‘a’	395.4	419.96	6.21
	‘b’	536.66	590.59	10.04
Solar	‘a’	95.45	95.58	≈0
	‘b’	78	78.229	≈0

Table 4.7 Comparison of fault currents supplied by wind and PV generators for double line to ground fault between phases ‘a’ and ‘c’ at bus 180

Type of source	Faulted phase/s	Peak fault current (A)		% error
		Balanced system	Un-balanced system	
Wind	‘a’	541.34	558.8	3.22
	‘c’	400	423.28	5.82
Solar	‘a’	89.67	91.2	1.7
	‘c’	109.62	109.36	≈0

Table 4.8 Comparison of fault currents supplied by wind and PV generators for double line to ground fault between phases ‘a’ and ‘c’ at bus 200

Type of source	Faulted phase/s	Peak fault current (A)		% error
		Balanced system	Un-balanced system	
Wind	‘a’	536.66	581.64	8.38
	‘c’	395.4	434.25	9.82
Solar	‘a’	78	78.25	≈0
	‘c’	95.45	95.65	≈0

4.6.3 Line to line fault

Similar to the above case, the line to line fault has been simulated between phases ‘a’ and ‘b’ and ‘a’ and ‘c’ at buses 180 and 200. The graphs showing the fault currents supplied by the DFIG and the PV system have been demonstrated in figure 4.3 below.

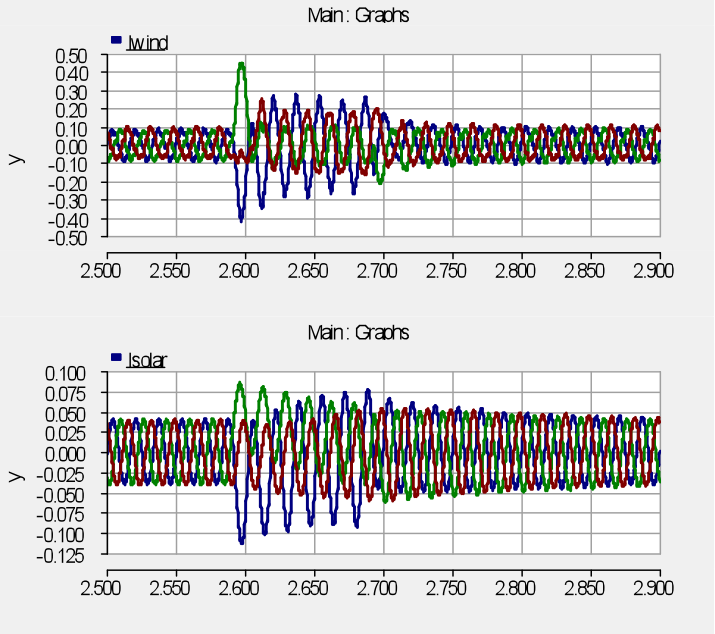

Figure 4.3 Fault current supplied by DFIG and the PV system during the fault at bus 180

The magnitude of peak fault currents for line to line faults between phases 'a' and 'b' and phases 'a' and 'c' at buses 180 and 200 have been presented in tables 4.9, 4.10, 4.11 and 4.12 respectively.

Table 4.9 Comparison of fault currents supplied by wind and PV generators for line to line fault between phases 'a' and 'b' at bus 180

Type of source	Faulted phase/s	Peak fault current (A)		% error
		Balanced system	Un-balanced system	
Wind	'a'	415.5	471.91	13.57
	'b'	446.9	420	6.01
Solar	'a'	113.116	112.156	0.84
	'b'	84.66	83.529	1.33

Table 4.10 Comparison of fault currents supplied by wind and PV generators for line to line fault between phases ‘a’ and ‘b’ at bus 200

Type of source	Faulted phase/s	Peak fault current (A)		% error
		Balanced system	Un-balanced system	
Wind	‘a’	407.01	484.90	19
	‘b’	423.85	432.49	2.03
Solar	‘a’	99.104	99.25	≈0
	‘b’	73.83	73.46	≈0

Table 4.11 Comparison of fault currents supplied by wind and PV generators for line to line fault between phases ‘a’ and ‘c’ at bus 180

Type of source	Faulted phase/s	Peak fault current (A)		% error
		Balanced system	Un-balanced system	
Wind	‘a’	446.9	426.91	4.47
	‘c’	415.5	512.41	23.32
Solar	‘a’	84.66	86.46	2.12
	‘c’	113.11	113.37	≈0

Table 4.12 Comparison of fault currents supplied by wind and PV generators for line to line fault between phases ‘a’ and ‘c’ at bus 200

Type of source	Faulted phase/s	Peak fault current (A)		% error
		Balanced system	Un-balanced system	
Wind	‘a’	423.85	442.65	4.43
	‘c’	407.01	524.689	28
Solar	‘a’	73.83	73.588	≈0
	‘c’	99.104	98.103	1.01

The figures 4.1 – 4.12 represent the fault current contributions from wind and solar generation for all types of asymmetrical faults. The fault studies have been carried out at two buses in the system and involve all the phase combinations for faults between two phases. The time of application of faults has been kept identical in both the balanced and unbalanced cases for all types of faults. The results show a significant difference in the fault currents for some types of faults.

CHAPTER 5: DISCUSSION AND CONCLUSION

5.1 Contribution of the thesis

The thesis is motivated by the need to carry out fault studies in distribution systems with distributed generation and to observe the impacts of the inherent unbalance in distribution systems on fault currents in the system. Fault currents at various buses in the distribution system govern the relay settings in the system. This work studies the extent of an impact a wind generator (DFIG) generating 1.25 MW and a 0.6 MW solar farm have on the fault current magnitudes of a 14 bus distribution system.

This thesis has simulated a 14 bus distribution system with a grid connected DFIG and a grid connected photovoltaic generator and observed the effect of unbalance in distribution systems on fault current magnitudes for various types of asymmetrical faults. This work has presented results showing that significant differences in the fault currents supplied by the distributed sources arise due to the unbalance that should be taken into account for system planning.

5.2 Conclusion

This thesis involves the modeling, control and fault simulations in a 12.47 kV, 14 bus distribution system in PSCAD software. The initial part of this work includes the modeling and control of a DFIG used for the purpose of wind generation. A detailed mathematical analysis of the rotor side and grid side converters has been shown and the implementation of field oriented control for both the converters has been presented. The d and q axis based flux and voltage has been used for the implementation of the control

scheme for both converters. The rotor side converter involves a two stage control with a current loop and a speed loop. The stator side converter uses the dc link voltage to control the real power exchange between the grid and the converter. The reference reactive power has been maintained at zero for both the converters. A small reactive power exchange still takes place due to the magnetizing current requirement of the machine. The graphs showing the steady state performance, under the implemented control, confirm the desired behavior of the DFIG in the system.

The second section involves the modeling and control of a three phase grid connected photovoltaic system in PSCAD. The PV array used is an inbuilt module in PSCAD based on the current – voltage equation mentioned in the introduction. A maximum power point tracker has been used to ensure the optimal operation of the PV array under any given solar insolation and cell temperature. A dc – dc converter has been used as part of this implementation. A simple P-Q control has been implemented for the three phase inverter for controlling the real and reactive power exchange between the grid and the PV system Similar to DFIG, the reference reactive power has been set to zero. The results presented at the end of chapter three confirm the steady state behavior of the grid connected photovoltaic system.

The last and the most important part of the thesis presents results showing the difference in magnitude of fault currents supplied by wind and solar generators with different levels of unbalance in the system. The faults have been simulated at two different locations in the system to confirm the effect of unbalance on the magnitude of the peak of the fault currents. The steady state voltages have been maintained within the

six percent regulation limits and no exaggerated values have been used in the system. The results presented show a significant difference in fault currents supplied by the DFIG. The percent difference in fault currents is found to be more for faults at bus 200 than at bus 180. The difference is much higher in ungrounded faults than ground faults. This difference in fault currents could affect the operation of protective equipment in the system resulting in events such as mal-coordination of protective equipment during a fault. Moreover, the wind and solar generation capacities have been constantly increasing. So, a higher difference in fault currents is expected for larger installed capacity of wind or solar generation. The grid connected photovoltaic system supplies comparable currents in both the cases. The reason for this behavior is the presence of a high step down transformer connecting the photovoltaic system to the grid that makes the presence of limited unbalance on the grid side almost absent on the terminals of the photovoltaic system.

5.3 Future work

In future, the effect of unbalance can be studied with much larger capacity of distributed generation installed in the distribution system. The source used in this study is connected to the distribution system through an inductance. The X/R ratio can be reduced to observe the magnitude of fault currents supplied by the distributed sources and the difference in magnitudes of fault currents under different levels of unbalance. A weak grid (low X/R ratio) also brings voltage boosters such as capacitors, autotransformers and FACTS devices into picture. The impact of unbalance in presence of these components will surely be different than the study presented in this thesis.

APPENDIX A

14 BUS DISTRIBUTION SYSTEM

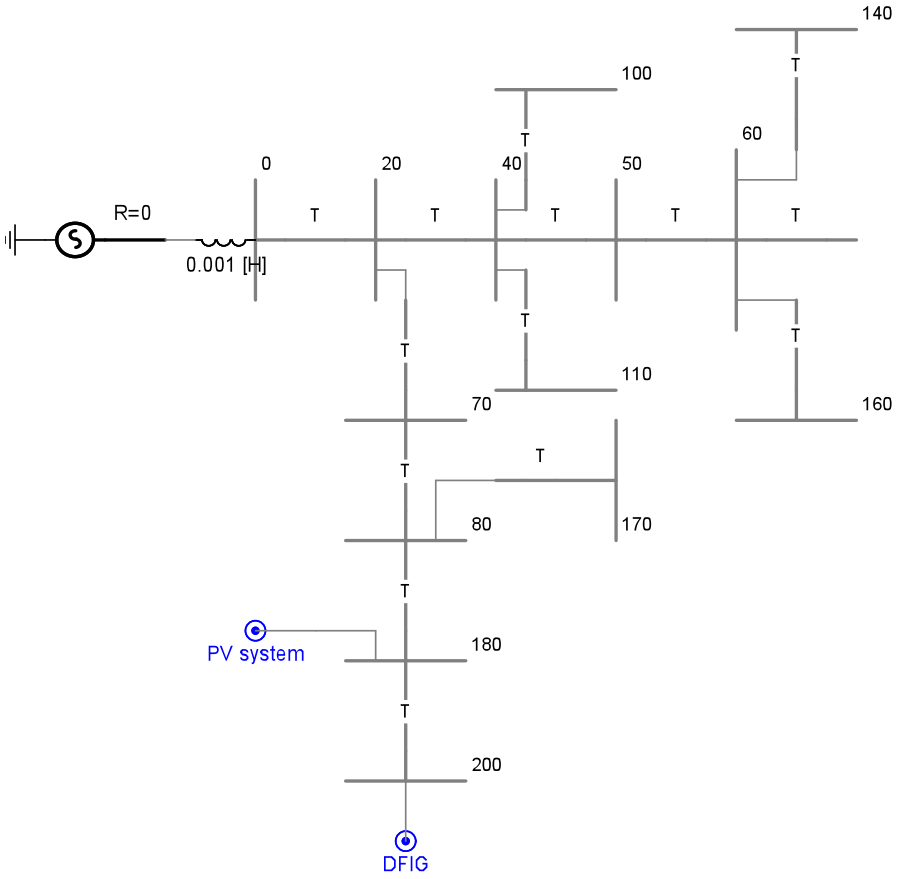

Figure A.1 14 bus distribution system with distributed generation

Figure A.1 shows the schematic of the 14 bus distribution system used for the study. Bus '0' represents the grid. The grid connected photovoltaic system is connected at bus 180 and the wind generation is connected at bus 200. Table A.1 lists the line length, phasing and conductor data for all the feeders in the system.

Table A.1 Transmission line parameters

Line Number	From Bus	To Bus	Line Length (Miles)	Phasing	Conductor Type and Code
1	0	20	1	ABC	A 336,400
2	20	40	1.45	ABC	B 336.400
3	40	50	1.15	ABC	A 336,400
4	50	60	1.3	ABC	B 336,400
5	20	70	0.6	ABC	B 336,400
6	70	80	0.9	ABC	B 336,400
7	80	180	1.05	ABC	A 4/0-6/1
8	40	100	0.4	ABC	A 4/0-6/1
9	40	110	0.3	ABC	A 4/0-6/1
10	60	140	1.1	ABC	A 4/0-6/1
11	60	160	0.75	ABC	A 4/0-6/1
12	80	170	1.6	ABC	A 4/0-6/1
13	180	200	0.4	ABC	A 4/0-6/1
14	200	DFIG	6.2138	ABC	A 4/0-6/1
15	180	PV	3.1069	ABC	A 4/0-6/1

There are two feeder configurations that have been used in the system and shown in the figure A.2 below. The dimensions mentioned in the figure are in feet.

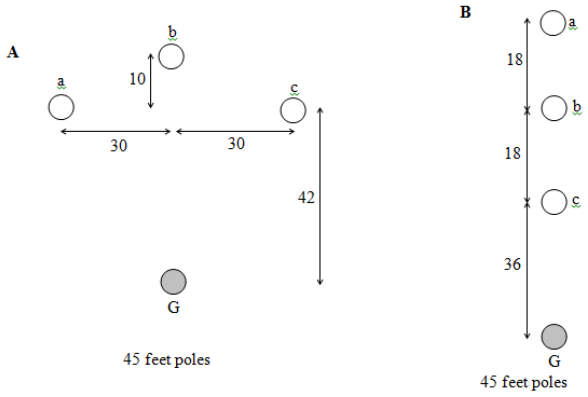

Figure A.2 Feeder configurations

The ground conductor configuration for all the feeders in the system is 'ACSR 4/0-6/1'. The conductor material and the number of strands for both the conductor codes used in the system have been mentioned in table A.2 below.

Table A.2 Conductor code, material and the number of stands

conductor code	material	number of strands
336,400	ACSR	26/7
4/0-6/1	ACSR	6/1

The loads at various buses in the system have been provided in table A.3.

Table A.3 System loading data

Node	P(kW)	Q (kVAR)
20	654	202
40	576	215
50	225	80
60	200	70
70	305	104
80	74	28
100	175	100
110	133	51
140	298	151
160	208	70
170	200	160
180	343	122
200	300	119

REFERENCES

[1] Varaiya, P.P.; Wu, F.F.;Bialek, J.W., "Smart Operation Of Smart Grid: Risk Limiting Dispatch ", Proceedings of the IEEE, Volume 99, Issue 1, Jan 2011, Page(s) 40-57

[2] Barker, P.P.;De Mello, R.W., "Determining The Impact Of Distributed Generation On Power Systems .I. Radial Distribution Systems", Power Engineering Society Summer Meeting, 2000. IEEE, Volume 3, Page(s) 1645-1656

[3] Reuters Article, "E.ON Completes World's Largest Wind Farm In Texas", 2009, URL: http://www.reuters.com/article/2009/10/01/wind-texas-idUSN3023624320091001

[4] Eurus Energy, "NRG Solar and Eurus Energy's Avenal Solar Facility Starts Generating Power", 2011, URL: http://eurusenergy.com/news/press-releases/eurus-energy-america/nrg-solar-and-eurus-energy%E2%80%99s-avenal-solar-facility-starts-generating-power/

[5] Energy Meteorology, "Grid Integration of Distributed and renewable Electricity Generation", URL: http://www.energy-meteorology.de/18011.html

[6] Thomas Ackermann, "Wind Power In Power Systems", ISBN 0-470-85508-8

[7] Ion Boldea, "Variable Speed Generators", ISBN 0-8493-5715-2

[8] Ryan konopinski, "Voltage Security Assessment With High Penetration Levels Of Utility-scale Doubly Fed Induction Generator Wind Plants", M.S Thesis, Dept. of ECE, Iowa State University, Ames, Iowa, U.S.A, 2009

[9] Paul C. Krause, "Analysis OF Electric Machinery", ISBN 0-471-14326-X

[10] Ramu Krishnan, "Electric Motor Drives: Modeling, Analysis, and Control", ISBN 0-13-091014-7

[11] Pena, R.; Clare, J.C.; Asher, G.M. "Doubly fed induction generator using back-to-back PWM converters and its application to variable-speed wind-energy generation", Electric Power Applications, IEE proceedings, Volume 143, Issue 3, May 1996, Page(s) 231-241

[12] Hosseini, S.H.; Sharifian, M.B.B.;Shahnia,F.; "Dynamic Performance of Double Fed Induction Generator for Wind Turbines", Electrical Machines and Systems, ICEMS, Proceedings of the Eighth International Conference on, Volume 2, Sept. 2005, Pages(s) 1261-1266

[13] Badrul H. Chowdhury; Srinivas Chellapilla; "Doubly-Fed Induction generator control for variable speed wind power generation", Electric Power Systems Research, Volume 76, Issues 9-10, June 2006, Page(s) 786-800

[14] Machmoum, F.; Poitiers, F.; Darengosse, C.; Queric,A.; "Dynamic Performances of a Double-fed Induction Machine for a Variable Speed Wind Energy Generation", Power System technology, 2002, Proceedings of PowerCon 2002, International Conference on, Volume 4, 2002, Page(s) 2431-2436

[15] Mahadanaarachchi, V.P.; Ramakumar, R.; "Simulation of Faults in DFIG-based wind farms", Power and Energy Society general Meeting, 2009. PES '09. IEEE, July 2009, Page(s) 1-8

[16] Muljadi, E.; Samaan, N.; Gevorgian, V.; Jun Li; Pasupulati, S.; "Short Circuit Current Contribution for Different Wind Turbine generator Types" Power and Energy Society General Meeting, 2010 IEEE, July 2010, Page(s) 1-8

[17] A. A. Girgis and S. M. Brahma, "Effect of distributed generation on protective device coordination in distribution system," in Proc. Large Eng. Syst. Conf., Halifax, NS, Canada, 2001, Page(s) 115–119

[18] S. M. Brahma and A. A. Girgis, "Development of adaptive protection scheme for distribution systems with high penetration of distributed generation," IEEE Trans. Power Delivery, vol. 19, no. 1, Jan. 2004, Page(s) 56–63

[19] Rajapakse, A.D.; Muthumani, D.; "Simulation Tools for Photovoltaic System Grid Integration Studies", Electric Power and energy Conference, IEEE, Oct. 2009, Page(s) 1-5

[20] Von Jouanne, A.; Banerjee, B.; "Assessment of Voltage Unbalance", Power Delivery, IEEE Transactions on, Volume 16, Issue 4, Oct. 2001, Page(s) 782-790

[21] E.B. Makram, M.A. Bou-Rabee, A.A. Girgis, Three-phase modeling of unbalanced distribution systems during open conductors and/or shunt fault conditions using the bus impedance matrix, Electric Power Systems Research 13 (1987) 173183.

[22] Martin C. Rodriguez Paz; Renato G. Ferraz; Arturo Suman Bretas; Roberto Chouhy Leborgne; "System Unbalance and Fault Impedance Effect on Faulted Distribution Networks", Computers and Mathematics with Applications, Elsevier, Volume 60, Issue 4; August 2010, Page(s) 1105-1114

[23] Gampa, Karunakar; Vemprala, Srinaga A.C.; Brahma, S.M.; "Errors in Fault Analysis of Power Distribution Systems Using Sequence Component Approach", IEEE Transmission and Distribution Conference and Exposition, April 2010, Page(s) 1-6

[24] Harley, R.G.; Makram, E.B.; Duran, E.G; "The Effects of Unbalanced Networks and Unbalanced Faults on Induction Motor Transient Stability" IEEE Transactions on Energy Conversion, June 1988. Vol. 3, No. 2: p. 398-403

[25] Muljadi, E.; Butterfield, C.P.; "Pitch-controlled variable-speed Wind Turbine Generation", IEEE Transactions on Industry Applications, Volume 37, Issue 1, Jan/Feb 2001, Page(s) 240-246

[26] Prabha Kundur; "Power System Stability and Control", ISBN 007035958X

[27] Marti, J.R.; "Accurate Modeling of Frequency-Dependent Transmission Lines in Electromagnetic Transient Simulations", Power Engineering Review, IEEE, Volume PER-2, Issue 1, Jan 1982, Page(s) 29-30